Electrocatalytic activity of sputtered Pt and Pt_3Pd_2 thin films for SO_2(aq) electro-oxidation

HS Kotzé

orcid.org 0000-0003-1079-5698

Dissertation submitted in partial fulfilment of the requirements for the degree *Masters of Science in Chemistry* at the North-West University

Supervisor: Prof RJ Kriek

Co-supervisor: Dr A Falch

Graduation May 2018

21722676

Acknowledgements

Firstly, I would like to thank my Creator without whom I, and the cosmos within which we live and study, would not have existed.

I would also like to thank the following people:

- My parents, Prof Awie Kotzé and Petro Reinders, who brought me into this world and who have supported me throughout my entire life with love, patience, advice and motivation
- My stepfather, Vernon Reinders, who taught me to follow my dreams and passion, and for all the support and love from the day we first met
- My aunt, Alta Kotzé, for all the support (especially financial, in the past two years with all the medical bills) and love throughout my life
- My sisters, Simoné and Melissa Reinders, for all their support and love, and who were always there for me when I needed someone to talk to
- My study leader, Prof Cobus Kriek, for all his help, advice, knowledge, and patience
- All my friends, who supported me throughout the good and bad times, and looked after me when it was needed
- My landlords (and extra pair of parents), Meyer and Leone van Rooyen, for all their love, hot meals, and the support during the days when I had to stay in bed
- My co-study leader, Dr Anzel Falch, for all the help and advice in the lab
- Dr Vasilica Lates, who taught me all the practical lab skills required in my field of study
- All the medical practitioners (especially the specialists), who diagnosed, treated and helped me to get back on my feet

I would also like to thank the following institutions, for the opportunity and funding which made this project possible:

NWU ®
NORTH-WEST UNIVERSITY
NOORDWES-UNIVERSITEIT
YUNIBESITI YA BOKONE-BOPHIRIMA

crb
CHEMICAL RESOURCE BENEFICIATION
CHEMIESE HULPBRONVEREDELING

****In memory of Meyer van Rooyen (1957/04/30 – 2017/11/25)****

Abstract

The ever growing demand for energy and worldwide focus on global warming have dictated the course of research in energy production for the past couple of decades, with much emphasis placed on the need for clean and renewable energy sources as an alternative to the traditional fossil fuels. Possible methods for a clean, renewable and environmentally friendly energy source are based on the production of hydrogen through electrolysis. These methods have drawn considerable attention, as hydrogen can be used in a fuel cell where it combines with oxygen to produce H_2O and electrical energy. The electro-oxidation of aqueous SO_2 to H_2SO_4 represents one of the most promising avenues for large scale hydrogen production. In this reaction, H_2O is split indirectly to produce hydrogen gas as a product. The attractiveness of this reaction lies in the fact that it occurs at a much lower standard potential (E^0 = 0.158 V) than direct water electrolysis (E^0 = 1.230 V).

Although the electro-oxidation of SO_2 appears to be a highly efficient method for splitting H_2O, experimental results show that a large overpotential is required to drive this reaction at acceptable rates. This extra energy input is mostly due to the sluggish electrode kinetics of the SO_2 electro-oxidation reaction. Therefore, the optimisation of this reaction through electrocatalyst development is of great importance. Most studies have been done using Pt as catalyst material, and relatively little research has been conducted on binary catalysts. In this study, binary Pt_xPd_y and Pt/Pd thin film catalysts were produced on glassy carbon supports with magnetron sputtering and compared to Pt to determine the viability of these binary electrocatalyst compositions as a replacement for pure Pt. The most promising Pt_xPd_y catalyst, as well as Pt, was also subjected to rapid thermal annealing to study the effect that annealing has on the performance of the electrocatalysts.

The electrocatalytic activity and stability of the various catalysts were determined with multiple electrochemical techniques, which included cyclic voltammetry, linear polarisation and chronoamperometry. Rotating disc electrode experiments were also conducted in order to determine the kinetic properties of the catalysts through the use of various analysis methods. Other techniques such as scanning electron microscopy coupled with energy dispersive X-ray spectroscopy, atomic force microscopy and X-ray diffraction were also employed to characterise various physical properties of the thin film electrocatalysts.

It was found that Pd was not as active towards the electro-oxidation of SO_2 when compared to Pt, and that Pd and Pd-rich binary catalyst compositions suffered from stability issues due to the dissolution of Pd in acidic media. However, it was determined that some of the Pt_xPd_y catalysts exhibited superior activity when compared to Pt as well as acceptable stability. Pt_3Pd_2 was found to be the most active binary catalyst and was thus used in further experiments alongside Pt. Physical characterisation of the catalyst thin films revealed that annealing caused various

changes in the structure and properties of the catalysts. Annealing was also shown to negatively impact the activity of the electrocatalysts; however, it did improve stability in some cases.

Tafel analysis of the data obtained from the rotating disc electrode experiments confirmed that annealing does indeed have a negative effect on catalyst activity. Kinetic parameters determined with Tafel analysis showed that while non-annealed Pt had the highest exchange current density, non-annealed Pt_3P_2 exhibited the lowest Tafel slope, and that for the SO_2 electro-oxidation reaction the Tafel slope appeared to be the most important kinetic parameter.

It was concluded that Pt_3Pd_2 is a promising replacement for Pt as catalyst material and that annealing has a positive effect on the stability of Pt_3Pd_2. Although annealing had a negative effect on the activity of the electrocatalyst thin films, this effect was much less pronounced on Pt_3Pd_2, and annealing could possibly be employed to improve the stability while retaining the activity of the binary catalyst, if the correct annealing temperature can be determined.

Keywords: SO_2 electro-oxidation, Electrocatalyst, Platinum, Palladium, Annealing, Activity, Stability, Rotating disc electrode, Tafel

Table of Contents

Table of Contents continued

Table of Contents continued

List of Tables

List of Figures

Abbreviations & Symbols

Abbreviation/Symbol	Description	Unit
$C_{R/O}$	Concentration of Reduced/ Oxidised Species	$mol.L^{-1}$
D_R	Diffusion Coefficient	$cm^2.s^{-1}$
E	Applied Potential	V
E_e	Equilibrium Potential	V
E^0	Standard Potential	V
i_0	Exchange Current Density	$mA.cm^{-2}$
I_k	Kinetic Current	mA
I_L	Limiting Current	mA
k^0	Standard rate constant	
v_R	Kinematic Viscosity	$cm^2.s^{-1}$
α	Symmetry Factor	
η	Overpotential	V
ω	Rotation Rate	$rad.s^{-1}$
A	Geometric Area	cm^2
E_a	Activation Energy	$J.mol^{-1}$
E_i	Onset Potential	V
E_p	Peak Potential	V
I	Current	mA
i	Current Density	$mA.cm^{-2}$
i_p	Peak Current Density	$mA.cm^{-2}$
n	Number of Electrons	
F	Faraday's Constant	$C.mol^{-1}$
R'	Resistance	Ω
R	Gas Constant	$J.K^{-1}.mol^{-1}$
$R^{2(1')}$	Coefficient of Determination	

T	Temperature	K
t	Time	s
Ar	Argon	
AFM	Atomic Force Microscopy	
CA	Chronoamperometry	
CE	Counter Electrode	
CV	Cyclic Voltammetry	
ECSA	Electrochemically Active Surface Area	cm^2
e^-	Electron	
H^+	Proton	
H_2	Hydrogen	
H_2O	Water	
H_2SO_4	Sulphuric Acid	
$HClO_4$	Perchloric Acid	
HyS	Hybrid Sulphur	
LHV	Lower Heating Value	
LP	Linear Polarisation	
N_2	Nitrogen	
NHE	Normal Hydrogen Electrode	
Pd	Palladium	
Pt	Platinum	
RDE	Rotating Disc Electrode	
RMS	Root Mean Square	
RTA	Rapid Thermal Annealing	
SO_2	Sulphur Dioxide	
SCE	Standard Calomel Electrode	
SDE	Sulphur Dioxide-Depolarised Electrolysis	
SEM/EDX	Scanning Electron Microscopy/ Energy Dispersive X-Ray Spectroscopy	

Std.Dev.	Standard Deviation
WE	Working Electrode
XRD	X-Ray Diffraction

1 INTRODUCTION

Sulphur dioxide is a major industrial pollutant that can cause severe health and environmental problems. It is produced by a number of different industries as well as through natural processes [1, 2], and minimising emissions of this toxic gas is of the utmost importance. The electrochemical oxidation of aqueous sulphur dioxide (SO_2) in concentrated sulphuric acid (H_2SO_4) solutions is referred to as SO_2-depolarised electrolysis (SDE) and it presents a possible method for a reduction in SO_2 pollution, and also utilisation of this pollutant to produce useful chemical compounds. This reaction also forms part of the hybrid sulphur (HyS) cycle, which is seen as one of the most promising processes for large scale hydrogen production [3, 4]. Due to the importance of both these applications considerable research has been conducted on various aspects of this reaction.

The usefulness of SDE lies in the fact that SO_2, a toxic pollutant, is converted to H_2SO_4 with the subsequent formation of hydrogen gas. Both these compounds are less harmful than SO_2 and are also useful as a chemical precursor and an energy carrier, respectively. Hydrogen is highly attractive as an energy carrier due to its high energy density (by weight) and the fact that it doesn't contain carbon. Besides its use as an energy carrier hydrogen is also used in extensive quantities for the production of ammonia through the Haber process in the fertilizer industry and for hydrocracking in the petroleum industry. Currently hydrogen produced from fossil fuels (natural gas, oil, coal) accounts for approximately 95% of global production, while water splitting processes, such as electrolysis, account for the remaining 5% [5, 6]. The SDE reaction represents a method for the indirect electrochemical splitting of water that requires much less energy compared to direct water electrolysis (E^0 = 0.158 V for SDE vs E^0 = 1.230 V for direct water electrolysis) [4]. The splitting of water can be accomplished by various methods (thermolysis, photolysis, electrolysis) and various reactions, and extensive research has been done on thermochemical and hybrid thermochemical sulphur-based water splitting cycles due to their high thermal efficiencies. Cycles such as these have the potential to produce hydrogen on an industrial scale (>100 000 kg H_2 per annum) [3, 7]. The most notable examples of sulphur based cycles are the sulphur iodine (S-I) thermochemical cycle and the HyS hybrid thermochemical cycle [8]. The HyS cycle is a two-step cycle that consists of an electrochemical (SO_2 oxidation to H_2SO_4 in a SDE electrolyser) and thermochemical (H_2SO_4 decomposition to SO_2) step.

Although the SDE reaction seems highly efficient in theory, experimental data shows that electrolyser performance is not yet up to acceptable levels. Much research has been conducted on the optimisation of the electrolyser with studies focusing on various aspects of this electrochemical process. A critical review by O'Brien *et al.* (2010) states that the mechanism of

the oxidation reaction has been studied extensively, specifically with regard to application in the HyS cycle, and that research relating to electrolyser optimisation (e.g. mass transfer issues and SO_2 cross over) is being conducted by various institutions. The review gives an overview about studies on electrode materials but the authors go on to state that relatively little research has been conducted on catalyst development [3].

A possible method of improving electrolyser efficiency is by developing catalysts that are more active toward SO_2 oxidation. Currently pure platinum is still regarded as the best catalyst for this process [3]. A number of different base and precious metals, as well as various forms of carbon, has been studied as electrode materials for SDE [9 - 14] and Pt, as well as Pd and Au, was consistently found to be far more active than the other metals, while carbon electrodes were deemed 'inactive'. Binary metal catalysts show potential for the development of electrode materials for SDE considering the use of binary and ternary catalysts in other applications (e.g. direct methanol fuel cells [15]) and the fact that this class of electrode materials has not been extensively studied for application in SDE. Certain binary metal catalyst compositions could display a higher activity than pure Pt, which translates to increased electrolyser efficiency and lower operating costs, and in the case of SDE also resulting in a reduction in catalyst cost due to the lower Pt content. By synthesizing various binary Pt_xM_y compositions and testing the electrodes' activity toward SO_2 electro-oxidation, active compositions can be identified and further studied to determine the thermodynamic and kinetic properties of the given catalysts. Thermal annealing could also be employed to determine the effect of thermal pretreatment on catalyst activity and stability. By comparing the results of all the data a conclusion can be drawn about the suitability of the various binary catalysts as potential replacements of pure Pt with regard to SDE.

2 LITERATURE STUDY

2.1 Overview of HyS cycle & SDE

As a result of the huge growth experienced over the last century in the global population and economy, energy demand is greater than ever and also not likely to decrease in the foreseeable future. The increase in energy production is placing strain on an already vulnerable environment and dwindling natural resource supply. This is not a new phenomenon and indeed a large part of research conducted in the past few decades has focused on developing clean ('green') processes as well as optimising existing processes to be more efficient and environmentally friendly.

The HyS cycle is an example of a clean process that is both sustainable and non-polluting. This hybrid thermochemical cycle was first proposed by the Westinghouse Electric Corp. in the late 1970s and is also referred to as the Westinghouse cycle [16 - 18]. This two-step cycle was originally proposed as a method to produce hydrogen (a clean fuel) using nuclear and solar power, which produces no pollutants and also prolongs fossil fuel reserves. Another advantage of the cycle is that the produced hydrogen and oxygen gases are of high purity, which is a requirement for fuel cells. The HyS cycle consists of two chemical reactions: the thermal degradation of sulphuric acid to sulphur dioxide to produce oxygen (Equation 1), and the electrochemical oxidation of dissolved sulphur dioxide to sulphuric acid and hydrogen (Equation 2). The net reaction for one cycle of reduction-oxidation of the sulphur oxide compounds is the splitting of a water molecule into hydrogen and oxygen gas (Equation 3) with a high efficiency (>40% based on the lower heating value (LHV) of H_2) [3, 7].

$$H_2SO_4 \rightarrow SO_2 + H_2O + \tfrac{1}{2}O_2 \quad (1)$$

$$SO_2 + 2H_2O \rightarrow H_2SO_4 + H_2 \quad (2)$$

$$H_2O \rightarrow H_2 + \tfrac{1}{2}O_2 \quad (3)$$

The electrolyser employed in the electrochemical step (Figure 2.1) has been identified as the main source of inefficiency in the cycle [3] and optimisation of this step is crucial for the eventual industrial application of this process [4, 7, 19]. While SDE is an integral part of the HyS cycle, it is important to note that the reaction is also very useful in itself. It consumes a major industrial pollutant (SO_2) to produce sulphuric acid and hydrogen gas, requiring much less energy than direct water electrolysis. The SDE reaction can be broken down into two half-cell reactions; in the anode compartment dissolved sulphur dioxide is oxidised to produce sulphuric acid, protons

and electrons (Equation 4), and in the cathode compartment hydrogen ions are reduced to produce hydrogen gas (Equation 5).

$$SO_2 + 2H_2O \rightarrow H_2SO_4 + 2H^+ + 2e^- \quad E° = 0.158 \text{ V vs. NHE} \quad (4)$$

$$2H^+ + 2e^- \rightarrow H_2 \quad E° = 0.000 \text{ V vs. NHE} \quad (5)$$

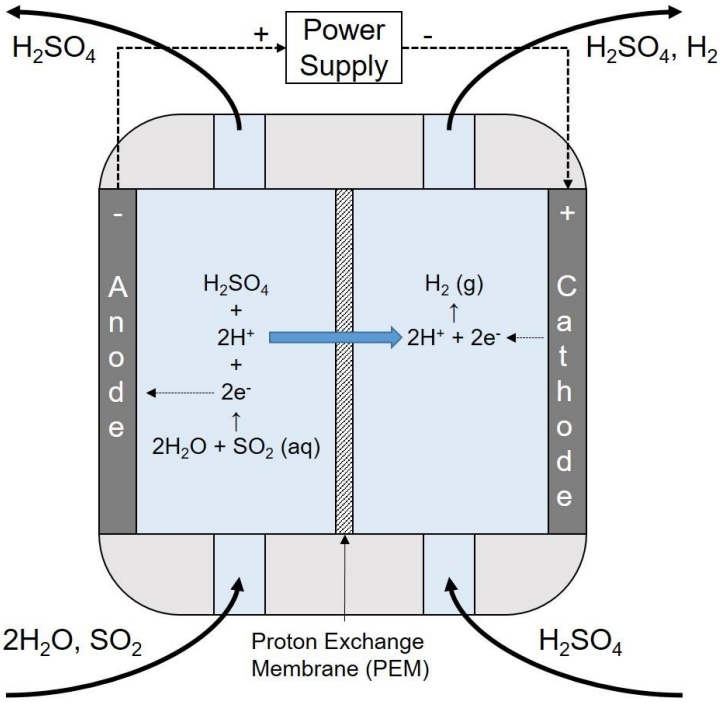

Figure 2.1: Schematic representation of SDE electrolyser (original Westinghouse design [3, 10, 20])

The standard cell potential (E°) for SDE is calculated to be 0.158 V vs. NHE [4, 17, 21], much lower than the 1.229 V required for direct water electrolysis. The low standard cell potential can be attributed to the fact that sulphur dioxide, dissolved in a concentrated sulphuric acid solution, depolarises the anode which facilitates oxidation. This phenomenon is also the origin of the reaction name, sulphur dioxide depolarised electrolysis.

Although SDE has the potential to produce large amounts of pure hydrogen with relatively small energy inputs, experimental data reveals many issues affecting the efficiency of this reaction and therefore leaves much room for improvement in various areas. The harsh operating conditions required in a SDE electrolyser (concentrated sulphuric acid and elevated temperatures) is one factor that causes a few problems. Some of the other key issues with the electrolyser are sulphur dioxide cross-over, mass transfer, cell overpotential, and catalyst cost and stability [3].

2.2 SDE electrochemistry

A major characteristic issue with SDE is the large anodic overpotential that is observed. Studies have shown that the anodic overpotential accounts for approximately half of the required applied voltage to produce a current density of 200 mA.cm^{-2} (total applied voltage = 0.85 V) [3, 22]. In one study, a constant current (200 mA.cm^{-2}) was applied to the cell, and the authors reported that an anodic and cathodic overpotential of 390 mV (η_a) and 50 mV (η_c) was generated at the individual electrodes [23]. The total applied potential (E) required to drive any electrochemical reaction is the combination of four components [19], shown in Equation 6.

$$E = E_e + \eta_a + n_c + iR' \quad (6)$$

E_e is the equilibrium potential (also known as reversible cell potential), η_a is the anodic overpotential, η_c is the cathodic overpotential, and the term iR$'$ represents the ohmic drop (due to the internal resistance of the cell). Cell overpotential (η) is defined as the difference between the applied potential (E) and the equilibrium potential (E_e) for the redox couple of interest, which is equal to the sum of the overpotentials at the anode and cathode and the ohmic drop, as shown in Equation 7. The equilibrium potential is calculated with the Nernst equation (Equation 8), where the parameter 'n' denotes the number of electrons transferred in the reaction, R is the ideal gas constant, T is the temperature (K) and F is Faraday's constant.

$$\eta = E - E_e = \eta_a + n_c + iR' \quad (7)$$

$$E_e = E^0 + \frac{RT}{nF} ln \frac{c_O}{c_R} \quad (8)$$

In order for a non-spontaneous electrolytic reaction like SDE to take place, the applied potential must be greater than the sum of the equilibrium potential, cell overpotential (sum of the overpotentials at the two electrodes) and the ohmic drop (Equation 6). Ohmic (iR$'$) drop is a result of the resistance the current encounters as it flows through the cell, and due to the fact that the current varies in most electrochemical experiments the value is not constant. Furthermore, since the resistance (R$'$) is determined by cell configuration and electrolyte concentration (i.e. characteristic of the electrolyte solution, not the reaction [24]), the effect of iR$'$ drop also varies between different electrochemical systems. Most modern electrochemical instrumentation (such as potentiostats) incorporate circuitry which allows for electronic compensation of this effect (iR$'$ compensation) [24].

2.3 SDE electrode kinetics & thermodynamics

While it is relatively easy to minimise energy loss due to iR drop (optimising cell design), overpotential presents more of a challenge. The equilibrium potential is defined as the potential of a redox couple in equilibrium, implying zero current (I = 0). In order to induce the flow of current through the system, an additional potential is needed on top of the equilibrium potential. This additional potential is represented by the cell overpotential and it consists of an anodic and cathodic component, the sum of which is the value of η. As is evident from the Butler-Volmer equation (Equation 9) the overpotential is a function of current density (i), which is in itself dependent on the catalyst surface area and current.

$$i = i_0 \left(e^{(1-\alpha)fn} - e^{-\alpha fn}\right) \quad (9)$$

i_0 is the exchange-current density, α is the transfer coefficient (also known as the symmetry factor) and f = F/RT. For SDE, the equation implies that anodic overpotential will increase as the current density increases and SO_2 concentration decreases [4]. Because the dissolved SO_2 concentration is influenced by temperature, pressure and H_2SO_4 concentration, it is obvious that overpotential is highly dependent on the reaction conditions. Furthermore, the Butler-Volmer equation shows that overpotential is also dependent on the exchange-current density (i_0), which is defined as the current that flows when the system is at equilibrium. Although the net current at equilibrium is zero, an anodic and a cathodic current (equal in magnitude but opposite in sign) are still present. The quantity of this parameter can be calculated with the equation given below (Equation 10).

$$i_0 = nFk^0 C_O^{*(1-\propto)} C_R^{*\propto} \quad (10)$$

Where n is the number of electrons that is transferred in a complete reaction, k^0 is the standard rate constant and $C_{O/R}^*$ is the concentration of the oxidised and reduced species (reactants and products) respectively, at the electrode surface. In the case where $C_O^* = C_R^* = C$, the equation can be simplified to $i_0 = nFk^0C$. It is clear from these equations that the exchange-current density is directly proportional to the standard rate constant, therefore higher i_0 values translate to fast kinetics. It can be concluded from the Butler-Volmer equation that overpotential is inversely proportional to exchange-current density, meaning higher exchange-current densities will result in lower overpotentials. The exchange-current density is highly dependent on the electrode surface, not only the electrode material (catalyst), but also the specific morphological attributes of the catalyst surface (e.g. crystallinity, adsorbed species) [24].

While improved electrode kinetics is a necessary requirement for the development of a suitable electrocatalyst for SDE, it is important to note that thermodynamics is of equal importance. A catalyst that displays fast kinetics but unfavourable thermodynamics (fast reaction rate that requires a large energy input) would be just as useless as a catalyst with sluggish kinetics but favorable thermodynamics. The interplay between these properties determines the theoretical efficiency of a process, which is in essence an indication of the amount of product formed per unit of energy supplied. In order for a catalyst to qualify as more active towards a specific process than its predecessor it should ideally display both improved kinetics and thermodynamics.

Although onset and peak potential (E_i and E_p, respectively) can be seen as 'thermodynamic variables', comparison between thermodynamic properties of catalysts should ideally include activation energy (E_a, kJ.mol^{-1}) in the analysis. Activation energy is defined as the energy barrier that has to be overcome before a reaction can take place. In other words, activation energy is the minimum energy that has to be introduced into a system to cause a chemical reaction, and it corresponds to the energy difference between the transition state with the highest energy and the reactants. This concept lies at the heart of catalysis, as a catalyst is defined as any substance (either a pure compound or a mixture) that increases the rate of a chemical reaction without being consumed in the process. With the use of a catalyst faster reaction rates can be obtained while using less energy, increasing the efficiency of the process. While various catalytic mechanisms exist, the common denominator is that the free energy of the transition state is lowered (smaller energy barrier). It is important to note that the total free energy of the reactants and products remains unchanged, only the free energy of the transition states is affected by the use of a catalyst [25]. In other words, a catalyst lowers the amount of energy needed to reach the transition state (lower activation energy), resulting in faster reaction rates at the same reaction conditions than the corresponding uncatalysed reactions. Although activation energy is frequently used to express the amount of energy required to initiate a reaction, it is however not the actual mathematical definition of this variable. The term 'activation energy' was first proposed by Svante Arrhenius as part of the Arrhenius equation (Equation 11), an equation formulated to determine the effect of temperature (T) on the reaction rate (k).

$$k = Ae^{-E_a/RT} \tag{11}$$

The parameter *A* is termed the pre-exponential or frequency factor and it has the same units as the reaction rate constant (k). The value of E_a can be calculated from a plot of ln k against 1/T, where the slope of the straight line is $-E_a/R$. Thus, a high activation energy implies that the reaction rate is highly temperature-dependent, while a value of zero implies that the reaction rate is not influenced by temperature. The activation energy can also be negative, indicating that the reaction rate decreases as temperature is increased. As is common in science, there are however exceptions to the rule in the sense that some reactions do not exhibit a linear relationship between

ln k and 1/T. In such cases, the value of E_a varies with temperature, and it can be determined with the equation given below (Equation 12).

$$E_a = RT^2(d(\ln k)/dT) \quad (12)$$

This equation is also valid for cases where activation energy is temperature-independent, as the equation simply reduces to the slope of a straight line (Arrhenius equation) [25].

2.4 Electrocatalyst activity & stability

The theory and equations above show that it is possible to increase the efficiency of the SDE electrolyser by developing catalysts with enhanced kinetic and thermodynamic properties. It also provides the parameters that define a catalyst's 'catalytic activity', enabling meaningful comparison between various catalysts when considering a specific electrochemical reaction. The value of these parameters (E_a and i_0) can be determined experimentally with electrochemical methods, but in both cases this requires multiple experiments at various reaction conditions (reaction temperature/electrode rotation speed) to calculate a single value. Considering the fact that a certain degree of repeatability is required and that most research on electrocatalysts includes several catalyst samples, it is not surprising that the determination of these parameters is excluded from most studies (time and budget constraints being always at play). When it is not possible/feasible to perform the experiments required to accurately calculate the values of E_a and i_0, other parameters, which are easier to determine experimentally, can be employed to quantify the thermodynamic and kinetic abilities of the catalyst. Peak current density (i_p), which is directly dependent on exchange-current density (Butler-Volmer equation), can be used as an indicator of the kinetic ability, while potential values such as onset and peak potential (E_i and E_p, respectively) relate to the thermodynamic attributes. Although the mathematical relationship between activation energy and the two potential parameters is not defined, intuitively it does make sense. Lower values of E_i and E_p indicate that less energy (lower potentials) is required to initiate and sustain the reaction (at the maximum rate) respectively, implying more favourable thermodynamics. Likewise, higher current densities indicate faster electrode kinetics, resulting in more products being formed while utilising the same amount of energy.

With regard to SDE, the above reasoning implies that any catalyst that displays higher current density (i, but i_0 can also be used if available) and/or lower potential (E_i and E_p) values when compared to Pt is catalytically more active towards SO_2 electro-oxidation. A catalyst's suitability for a certain reaction should however not be determined employing activity alone. While efficiency

is one of the most important parameters when considering the feasibility of a process, the stability of the catalyst also plays an important role. A catalyst with a high activity and low stability can result in increased operating costs when compared to a catalyst with a low activity and high stability, depending on the catalyst material and reactor design. The stability of a catalyst is of great importance in SDE due to the harsh operating conditions in the electrolyser and the fact that noble metals are usually employed. This is part of the reason why pure Pt is still considered to be the best catalyst for SDE. Few electrode materials can survive the harsh conditions required for SDE (elevated temperature and high sulphuric acid concentration), and developing catalysts with a higher degree of stability than Pt would likely be more complex than improving the catalytic activity. For processes such as SDE, where catalyst stability is already an issue [3], developing catalysts to improve efficiency can be challenging as any increase in activity will be rendered meaningless if there is a decrease in stability.

It should be noted that the term 'stability' refers to the life-time of the catalyst and not the thermodynamic stability of the system. While thermodynamic stability is a precisely defined parameter, there is no generally accepted parameter to quantify the stability of a catalyst. Although the term 'stability' appears in many papers, it is usually not well defined and often used interchangeably with the term 'durability'. In the most general sense, stability refers to how well a catalyst retains its physical integrity and catalytic activity over time. Thus, a catalyst that lasts for 5 hours would be defined as being more stable than a catalyst that lasts only 2 hours. In electrocatalysis, current density or potential (depending on the type of cell) is usually employed to assess the stability of the catalyst [26]. For galvanic cells (e.g. fuel cells), galvanostatic polarisation can be used to monitor the change in cell potential, while potentiostatic polarisation is employed in electrolytic cells to determine current decay. In both cases the 'performance' of the cell is monitored over a certain amount of time. For electrolytic cells (i.e. SDE electrolyser), the decay in current density (at a specific potential) is measured over time, as the current produced is directly proportional to the amount of product formed at the electrode surface. A requirement for the validity of this method is to maintain the reactant concentration (dissolved SO_2) at a fixed value for the duration of the experiment. By calculating the percentage decrease in catalytic activity for a certain amount of time, or determining the time it takes to reach a certain percentage value, a meaningful comparison between catalyst stability is possible. Although this method provides an indication of the long-term performance of a catalyst, it does not provide any information about the degradation mechanisms that causes the loss of catalytic activity. Catalyst poisoning, loss of active area, electrodissolution and various other phenomena can cause a decrease in activity [24, 26]. Determining which mechanisms are present in a certain process, as well as their individual contributions to the observed decrease in activity, is however very complex and beyond the scope of this study.

2.5 Electrocatalyst development

The activity and stability (as well as other properties) of electrocatalysts can be determined experimentally through various electrochemical techniques, all of which require electrodes incorporating the specific catalyst materials. Despite substantial variations in size and geometry, all electrodes can be defined as either bulk or thin film (substrate supported) electrodes. A bulk electrode consists solely of the catalyst material (e.g. polycrystalline Pt disc), while a supported electrode consists mainly of an inert support material core with only a layer of the catalyst material (thin film) covering the electrode-electrolyte interface (e.g. Pt nanoparticles on graphite support).

The use of bulk electrodes is largely restricted to the study of pure metal catalysts, of which a variety can be acquired from electrochemical vendors. This can be ascribed to the fact that few research facilities possess the resources and instrumentation required to produce such electrodes, especially when novel materials such as bimetallic catalysts are employed. Although this necessitates the use of substrate supported electrodes (in most cases where complex catalysts are studied), the prevalence of these electrodes in electrocatalysis research is most likely a result of the substantially lower material cost, as well as possible performance increases this type of electrode design offers [27]. Considering the fact that electron transfer only takes place at the electrode-electrolyte interface, catalytic material is only required on the part of an electrode's surface that is in direct contact with the electrolyte (heterogeneous catalysis). Theoretically, thin film electrodes are comparable to their bulk electrode counterparts, providing that the support material is inert and does not impede the flow of electric current (high chemical stability and conductivity) [24]. Carbon, in its various forms, is most often employed as support material (substrate) due to its excellent chemical stability and conductivity as well as the fact that it has a large specific surface area [27, 28]. Examples of carbon supports include graphite, graphene, various carbon nanostructures and glassy carbon (GC), which were employed in this study. Owing to its multiple advantageous properties (hardness, small pore sizes, low permeability to liquids and gases and a large usable potential range), glassy carbon is widely employed as support material [29, 30].

In practice, thin film electrodes frequently exhibit vastly different properties than their equivalent bulk electrodes. This can be attributed to the fact that the chemical and physical properties, and by extension also the electrochemical properties, of the surface layer atoms are not only dependent on the elemental composition, but also on the chemical and physical attributes of the layers beneath. This again highlights the fact that the electrochemical behaviour of a catalyst is highly dependent on the electrode surface, and not only the elemental composition [24]. There is also substantial differences between thin film electrodes of the same catalytic material, which

is a result of different film thicknesses, support materials and deposition techniques employed in electrocatalysis research. It should be noted that 'thin film' is not a precisely defined term, as electrodes with only a few nanometers of catalyst and electrodes incorporating micrometers or more of catalyst are both referred to as thin film electrodes. Catalyst materials can be deposited on supports employing a wide variety of chemical (electroplating, chemical vapour deposition) or physical (physical vapour deposition) techniques.

Physical vapour deposition techniques are widely applied to the manufacture of thin films (not only for electrocatalysis), and the multitude of methods available ensure that virtually any catalyst material can be deposited on a wide variety of supports. Examples include cathodic arc deposition, evaporative deposition, electron beam deposition, pulsed laser deposition and sputter deposition, with each of these techniques offering a subset of individual methods. Magnetron sputtering (employed in this study), alternatively known as (ion) plasma sputtering, is one of the most prevalent methods and it allows for rapid (i.e. high productivity), effective and uniform deposition of metal particles over a large area [28, 31].

2.6 Electrocatalyst evaluation

After the catalysts have been deposited on electrodes they can be characterised in an electrochemical cell that is coupled to appropriate electrochemical instrumentation (usually a potentiostat). In this study a three-electrode cell coupled to a single channel potentiostat was employed, which is the standard setup for most electrochemical experiments (Figure 2.2). This configuration incorporates a third electrode in the cell, in addition to the anode and cathode. Depending on the electrochemical reaction being studied, the anode and cathode are alternatively termed the working electrode (WE) and counter electrode (CE, also referred to as the auxiliary electrode). The half-cell reaction of interest is located on the WE, with the other half-cell reaction occurring on the CE. In SDE, the half-cell reaction being studied (SO_2 oxidation) is an anodic reaction, and as a result the WE is considered the anode and the CE the cathode. All the electrodes are coupled to a potentiostat, an instrument that controls the potential between the WE and CE so that the potential, as measured between the WE and reference electrode (RE), corresponds to the value specified in the software. In this configuration current is passed between the WE and CE, while the potential of the WE is measured relative to a well-defined redox pair (RE), which is contained in a separate cell that is in electrical contact with the solution (i.e. a salt-bridge, usually a sintered/fritted glass separator). By connecting the RE to a high impedance input that prevents the flow of significant current through the electrode, the potential can be

measured (and thus also controlled) with higher accuracy. The reasoning behind this being that because negligible current flows through the RE, the contribution of Ohmic drop to the total current (Equation 6) is decreased [24].

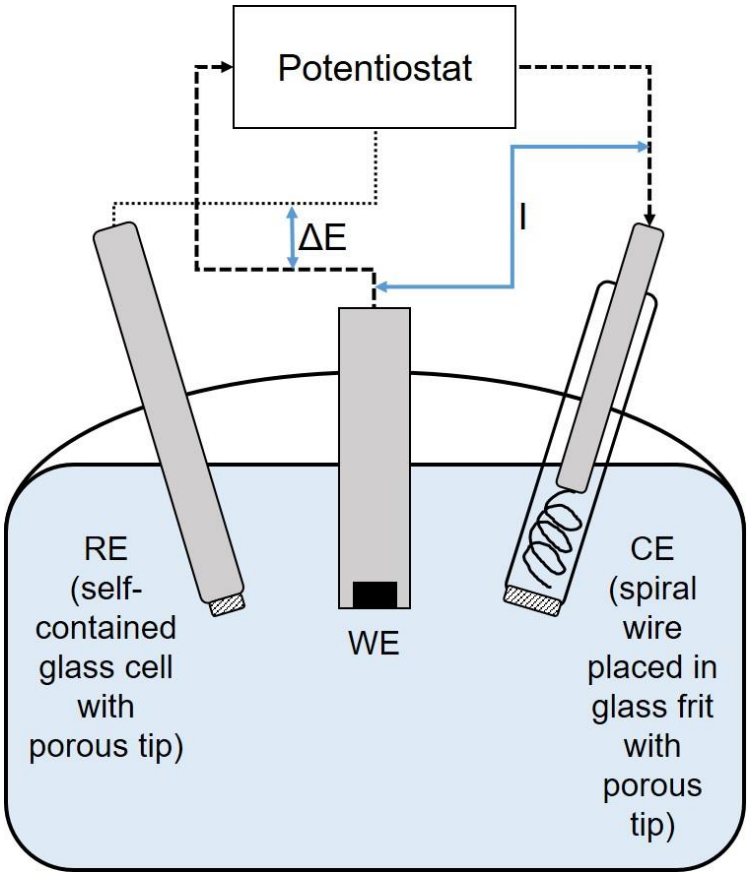

Figure 2.2: Schematic representation of a three-electrode cell

The three-electrode cell setup allows for the determination of various fundamental electrochemical properties relating to the working electrode material (catalyst), providing a more in-depth view than electrolysers and fuel cells (which are scaled up, 'applied' designs of the standard electrochemical cell). Owing to the fact that modern potentiostats are coupled to computers and that they also function as galvanostats (controls current), a wide array of electrochemical techniques are available to the researcher. In this study, potentiometric techniques (potential is controlled while current is measured as a function of another variable), are employed to determine catalyst activity and stability towards SO_2 oxidation. Activity is determined by means of linear sweep voltammetry (LSV), commonly referred to as linear polarisation (LP), a technique where current is measured as a function of potential (varied at a specified rate between two potential values). For an anodic reaction such as SDE, the potential is scanned from a lower potential (E_{Low}) to a more positive potential (E_{High}). Chronoamperometry

(CA) is employed to evaluate stability (also known as potentiostatic polarisation, see Section 2.4), and it involves applying a constant potential and measuring the current as a function of time.

Prior to these experiments a procedure known as preconditioning is performed, which is required to 'activate' the electrode. This consists of cycling the electrode between two potential limits (E_{Low} and E_{High}) in an electrolyte solution, a technique known as cyclovoltammetry (CV, identical to LSV except potential is cycled backwards and forwards multiple times). By cycling the electrode consecutively between potentials that includes metal oxide formation (more positive potential) and reduction (less positive potential), the electrode surface is altered in a manner that improves reproducibility. Specifically, in the case of a Pt catalyst in SDE, preconditioning is a requirement to ensure significant SO_2 oxidation [11].

An example of a LP curve is shown in Figure 2.3, indicating the data points corresponding to the activity parameters (E_i, E_p, I_p). In the second part of this study, rotating disc electrode (RDE) experiments are performed in order to determine exchange-current density (i_0). These experiments also employ linear polarisation, which is performed while the WE rotates at a specified rate. Data acquired at several rotation rates can be analysed through various methods to determine i_0, as well as other parameters. The data generated by RDE experiments, and the methods used to analyse it, are discussed in Chapter 4.

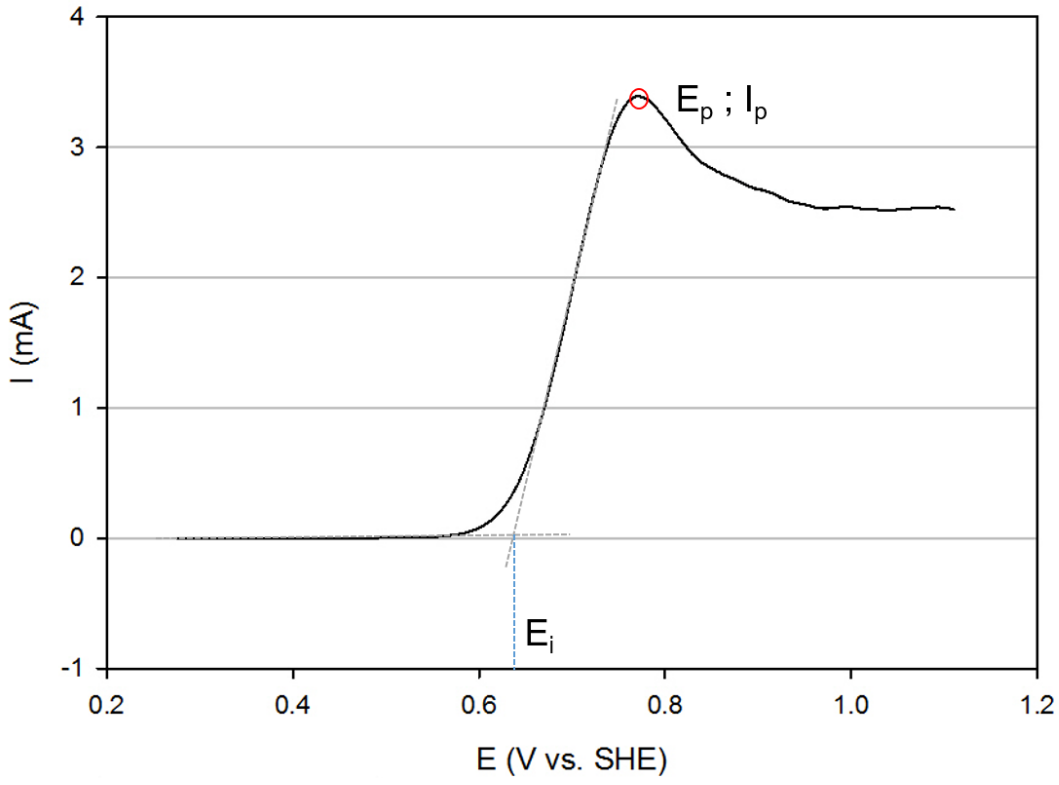

Figure 2.3: Typical linear polarisation (LP) curve for an anodic reaction

2.7 Electrode surface

As mentioned previously, the activity of an electrocatalyst is highly dependent on the electrode surface. After a catalyst has been deposited on a support, the surface of the electrode can be altered by either physical (e.g. heating) or chemical (preconditioning, adsorbed species) processes. Adsorbed sulphur species is of great importance in SDE due to the substantial effect it has on SO_2 oxidation. At potentials below 0.450 V dissolved SO_2 is reduced to elemental sulphur, resulting in a layer of adsorbed sulphur on the electrode surface (Equation 13) [14].

$$SO_2(aq) + 4H^+ + 4e^- \rightarrow S(s) + 2H_2O \qquad E^\circ = 0.450 \text{ V vs. NHE} \qquad (13)$$

This process is referred to as sulphur modification, and it has been conclusively proven to enhance Pt electrodes' activity towards SO_2 oxidation [3, 14, 32]. The magnitude of this effect is dependent on the extent of sulphur coverage, with excessive sulphur reduction resulting in decreased activity [32]. Consequently, the lower potential limit (E_{Low}) has a significant influence on the observed activity of Pt electrodes, as it directly determines the amount of adsorbed sulphur on the electrode surface. The effect of sulphur modification on the SO_2 oxidation activity of other electrode materials is largely unknown. Sulphur modification has been studied on Au and Pt electrodes, with results indicating that the catalytic activity of Au is not significantly influenced by sulphur modification [7, 14].

The surface of an electrode can also be altered with non-electrochemical methods, which are performed prior to the electrochemical experiments. In this study, electrodes are subjected to elevated temperatures (annealing) following the deposition of the catalyst layers. When a metal layer is heated to high enough temperatures (dependent on elemental composition) the atoms in the layer rearrange, causing a change in the surface structure. Some of the surface properties that can be altered with annealing include crystallinity and grain size, and this process has been shown to improve electrocatalyst performance for other reactions [33]. Although a number of studies on the annealing of various thin films has been conducted, the effect of annealing on Pt electrodes for SO_2 electro-oxidation remains largely unknown.

2.8 Previous work on catalysts for SO_2 oxidation

Platinum is generally accepted to be the most suitable catalyst for SDE [3]; however, a number of other metals have been studied as electrocatalysts for this reaction. These include Pd, Au, Ru,

Re, Ir, and Rh [9 - 14]. In each study Pt was tested along with the other metal catalyst(s) under a certain set of conditions. Lu and Ammon (1980 & 1982) included Pt, Pd, Au, Ru, Re, Ir and Rh in their study and found that Pd was a better electrocatalyst than Pt for SO_2 oxidation [9, 10]. In a more recent study that tested the activity and stability of Pt and Pd as electrocatalyst for SDE the authors however concluded that Pt provided the highest catalytic activity [13]. O'Brien *et al.* (2012) compared Au and Pt electrodes and found gold to be quite active toward SO_2 oxidation [14]. Carbon materials were also studied as electrode materials, but proved to be relatively inactive towards SO_2 oxidation [9, 12]. It should be noted that electrode preparation and preconditioning, as well as cell conditions (H_2SO_4 and SO_2 concentration, temperature), are different in each study. Comparing the results to draw a definite conclusion of which metal is the best catalyst is therefore difficult, especially since it is considered that even varying H_2SO_4 concentration can have an effect on the reaction mechanism of a given metal catalyst [3].

Very few comprehensive studies have been conducted on binary metal catalysts for SDE. Lee and Langer (1994) studied Pt electrodes modified with small amounts of Al and results exhibited a large increase in electrode performance with small amounts of Al (1-10%) incorporated in the Pt electrode [17]. Xue *et al.* (2014) investigated several Pt-based bimetallic catalysts (Pt-M, where M = Pd, Rh, Ru, Ir, Cr) and found Pt-Cr to be the most active composition, with a Pt:Cr atomic ratio of 1:2 exhibiting activities comparable to that of Pt [19].

After considering the results of these studies, the choice was made to use Pd as the second metal in this study. This was based on the fact that there are conflicting results on the suitability of this metal for SDE. While both studies prove that Pd is active towards SO_2 oxidation, the authors differ on Pd's activity compared to that of Pt [9, 13].

2.9 Focus of the study

Considering the amount of research conducted on various aspects of SDE, mostly relating to its use in the HyS cycle, the fact that pure Pt is still regarded as the best catalyst for this process clearly shows that much work remains on catalyst development. Furthermore, since limited information is available on the majority of electrode materials, there is considerable disagreement about the viability of these catalysts for SDE.

In this study, the activity of Pt, Pd and several Pt_xPd_y electrocatalysts will be determined in order to draw a conclusion on the suitability of the pure metals, as well as the binary Pt_xPd_y compositions, for application in SDE. Following the successful completion of these goals, Pt and

the most active composition of P_xPd_y will be subjected to annealing at various temperatures to determine its effect on catalyst activity and stability. An attempt will also be made to determine the exchange current density (i_0) as a fundamental kinetic parameter of the annealed and non-annealed electrodes so as to enable comparison of the catalysts' inherent activity towards SO_2 electro-oxidation.

3 EXPERIMENTAL

3.1 Electrode preparation

Glassy carbon (GC) disks (5 mm diameter, SIGRADUR® G from HTW) were used as electrode support material. Catalyst layers were deposited on GCs employing plasma sputtering – a physical vapour deposition technique. Prior to sputtering the GCs were polished with a polishing kit from Pine Research Instrumentation, and then cleaned by ultrasonication in various solvents. Polishing was done by placing the GC in a Teflon electrode holder and physically moved in a figure-of-eight (25 cycles) over the polishing media while light pressure was applied. This was done in a stepwise method on clean nylon cloth first, followed by microcloth with 1 µm diamond paste (Struers DP-Paste M) and lastly a separate microcloth with 0.05 µm deagglomerated alumina suspension (Allied High Tech Products Inc.). The polished GCs were rinsed with deionised H_2O (Millipore Milli-Q ultrapure water system; 18.2 MΩ.cm) to remove any excess alumina suspension. The GCs were then cleaned by stepwise ultrasonication (15 min) in toluene (Minema; purity > 99.5%), followed by ethanol (Labchem; purity > 99.0%), deionised H_2O, and isopropanol (Labchem; purity > 99.7%). After the final ultrasonic cleaning the isopropanol was decanted and the GCs dried with a stream of N_2 (Afrox; purity > 99.999%) and immediately transferred to the sputtering tray. The catalysts were then sputtered onto the polished GCs with the sputtering apparatus (PVD Products).

Table 3.1: Parameters employed in the sputtering process

(Base pressure = 5×10^{-7} Torr, Chamber pressure = 8 mTorr, Ar flow rate = 0.015 $L.min^{-1}$)

Catalyst	**Theoretical fraction**		**Power (W)**		**Time (s)**
	Pt	Pd	Pt	Pd	
Pt	1	0	50	0	340
Pt_3Pd_2	0.6	0.4	50	22	207
Pt_2Pd_3	0.4	0.6	62	60	111
Pt_1Pd_4	0.2	0.8	24	60	148
Pt_1Pd_9	0.1	0.9	17	90	110
Pd	0	1	0	50	225

The thickness of the catalyst layers was kept constant at 60 nm, which was confirmed by the built-in quartz crystal microbalance. For the first part of the study, six different catalyst compositions were sputtered; Pt, Pd, Pt_3Pd_2, Pt_2Pd_3, Pt_1Pd_4 and Pt_1Pd_9. In the case of the binary compositions (Pt_xPd_y), the variables (x and y) represent the atomic ratio of the constituent elements. The settings employed during the sputtering process, subsequent to calibration, are shown in Table 3.1. The development of this process forms part of a previous study conducted by the research group [34].

3.2 Surface characterisation

Several analytical methods were employed in various stages to characterise the catalyst layers. Scanning electron microscopy coupled with energy dispersive X-ray spectroscopy (SEM/EDS) was performed on all catalysts to determine composition and to give a visual representation of the electrode surfaces. This enabled a comparison between the theoretical and experimental molar ratios of the sputtered binary compositions, and provided confirmation that the sputtering process was successful. The analysis was performed in moving average mode with a FEI Quanta FEG 250 SEM and integrated XMax 20 EDS system (Oxford Instruments).

In order to determine changes in crystallinity due to the annealing process, X-ray diffraction (XRD) analysis was performed on the annealed electrodes and their non-annealed counterparts. A PANalytical X'Pert Pro was employed for this analysis.

Atomic force microscopy was employed to map the catalyst surfaces and quantify the roughness in order to determine the effect of annealing on the surface morphology. The data generated by the Nanoscope V Multimode was analysed with Nanoscope Analysis software (Veeco).

Besides mounting the electrodes on holders, no specialised sample preparation was required for any of the techniques.

3.3 Rapid thermal annealing

3.3.1 Annealing oven

In order to induce physical changes in the catalyst layers, electrodes were subjected to elevated temperatures under an inert Ar (Afrox; purity > 99.999%) atmosphere. While annealing normally consists of long temperature programs, this study employed a rapid thermal annealing (RTA) oven (AccuThermo AW610), which allows for rapid controlled heating (up to 200 $°C.s^{-1}$) and cooling (uncontrolled) in short temperature programs (5 min). Objects are heated in a sealed

chamber by means of high-intensity electromagnetic radiation (21 kW tungsten halogen lamps) and the entire process is controlled by a computer with proprietary software (Allwin 21 Corp.), shown in Figure 3.1. The temperature profiles are created in the software and is fine-tuned by adjusting several variables until the real (experimental) temperature matches the model temperature in a reproducible manner.

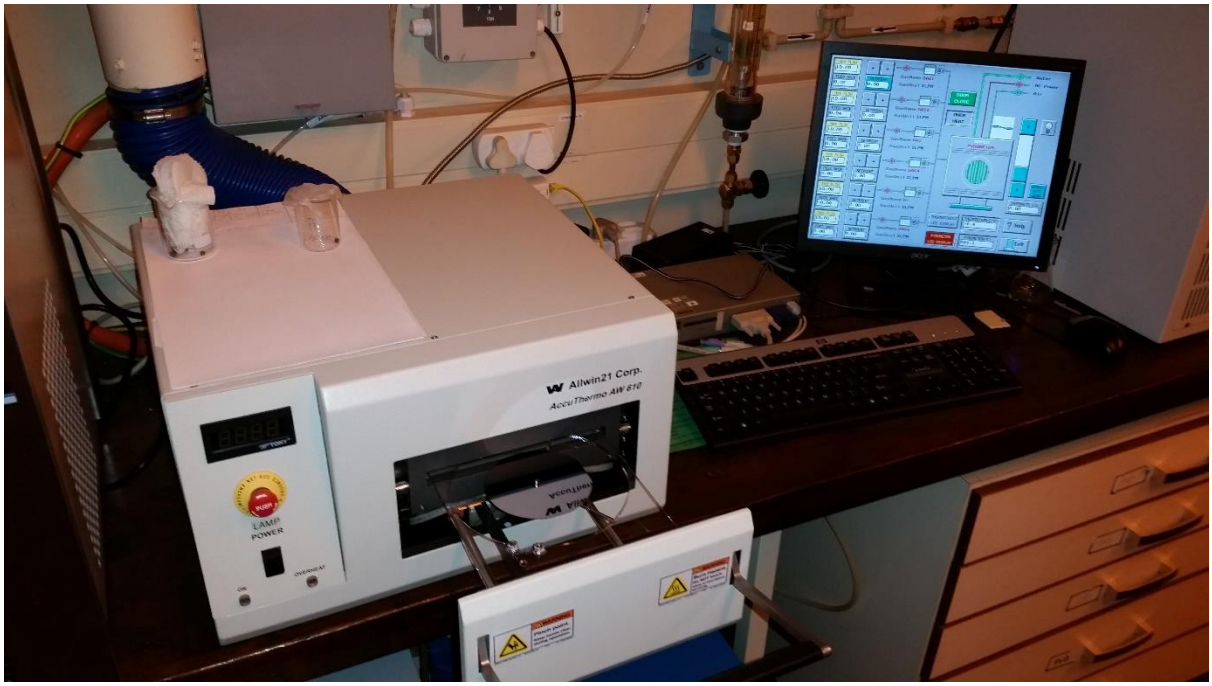

Figure 3.1: AccuThermo AW 610 RTA oven

3.3.2 Temperature program development

Four temperature programs were created for this study: 600, 700, 800 and 900 °C (898.15, 998.15, 1098.15 and 1198.15 K, respectively). The programs were identical in temperature profile except for the last steady state temperature (T_{High}) in the program. The variables employed in the temperature program (900 °C) and the corresponding temperature profile are shown in Table 3.2 and Figure 3.2, respectively.

Table 3.2: RTA parameters for 900 °C temperature program (T_{High} indicated with *)

No.	Function	Time (s)	Temp/Intn (°C/%)	Steady Intn Factor	Gas 1 Ar (SLPM)
1	Delay	35.0	0.0	1.00	10.0
2	Intn	14.0	18.0	1.00	5.0
3	Steady	10.0	450.0	0.80	5.0
4	Ramp	10.0	500.0	0.90	5.0
5	Steady	20.0	500.0	0.80	5.0
6	Ramp	15.0	900.0*	0.90	5.0
7	Steady	30.0	900.0*	0.80	5.0
8	Delay	120.0	0.0	1.00	10.0
Universal parameters					
Delay = 1.20		Gain = 0.60		Sensitivity = 0.65	

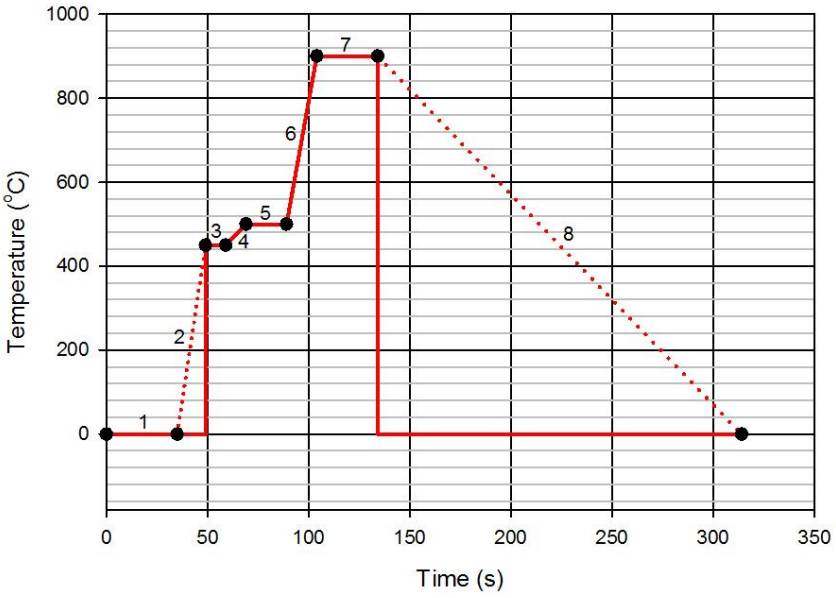

Figure 3.2: Temperature profile of 900 °C showing the individual steps in the temperature program

The numbers in Figure 3.2 correspond with the step numbers in the temperature program (Table 3.2), with the solid red line representing the program as seen in the software while the dotted line shows the approximate actual temperature when the program is executed. The intensity (Intn, no. 2) and delay steps (no. 1 and 8) represent the time periods where temperature is not actively controlled. In the delay phases no power is being supplied to the lamps (0%) and the gas flow (Ar) is increased to 10 Standard Litres Per Minute (SLPM), which purges the chamber and indirectly also cools the chamber. The purpose of the intensity phase (18% lamp power for 14 s) is to heat the sample to above 450 °C, which is the lower point in the pyrometer's effective temperature range. The oven permits the use of either the pyrometer or a thermocouple (which can accurately measure lower temperatures); however, the thermocouple has to be removed for annealing experiments above 650 °C. In order to increase reproducibility, the steady state at 450 °C (no. 3) was included to allow the temperature to stabilise before the sample was heated in a controlled manner.

After the temperature profiles had been programmed into the software, optimisation of the global parameters was required to ensure that the programs executed successfully each time. This required multiple runs with an electrode present in the chamber, with the first couple of program executions resulting in incomplete runs. By assessing the data and identifying the steps that caused the failure, the global parameters were adjusted in small increments (0.05) from their standard value (1.00 for all three parameters). The gain was adjusted first, followed by the sensitivity (which itself is a function of gain) and lastly the delay. When the temperature programs could be executed consistently without failure, the parameters were adjusted in smaller increments (0.01) until maximum accuracy of the real temperature was obtained. In all, the development of reproducible and accurate temperature programs entailed countless trial-and-error runs, requiring several weeks.

3.4 Electrochemical setup

3.4.1 SO_2 oxidation

A standard three-electrode electrochemical cell (125 mL) with a Pt wire counter electrode (CE, Pine Research Instrumentation) in a glass frit and a saturated calomel reference electrode (SCE, Radiometer) was used for all electrochemical experiments in this study. Experiments were performed employing EC-Lab software coupled to a VSP potentiostat (Bio-Logic). All potential (E) values in this paper are given with respect to the normal hydrogen electrode (NHE). An offset of +0.241 V (E vs NHE) was used to convert the values obtained in EC-Lab ($V_{NHE} = V_{SCE} + 0.241$ V). The working electrode (WE) was attached to a rotator coupled with a MSRX speed controller

(Pine Research Instrumentation) to facilitate controlled rotation of the electrode. Temperature was kept constant at 25.0 °C (298.15 K) for all experiments with a Julabo F12 ED refrigerated temperature control unit. The setup employed in these experiments is shown in Figure 3.3.

The accuracy of the reference electrode was periodically checked by measuring the potential against a 'standard' reference electrode in a 1 M KCl (Merck; purity > 99.0%) electrolyte solution. The 'standard' is an identical SCE reference electrode that is exclusively used for the purpose of determining the accuracy of other reference electrodes.

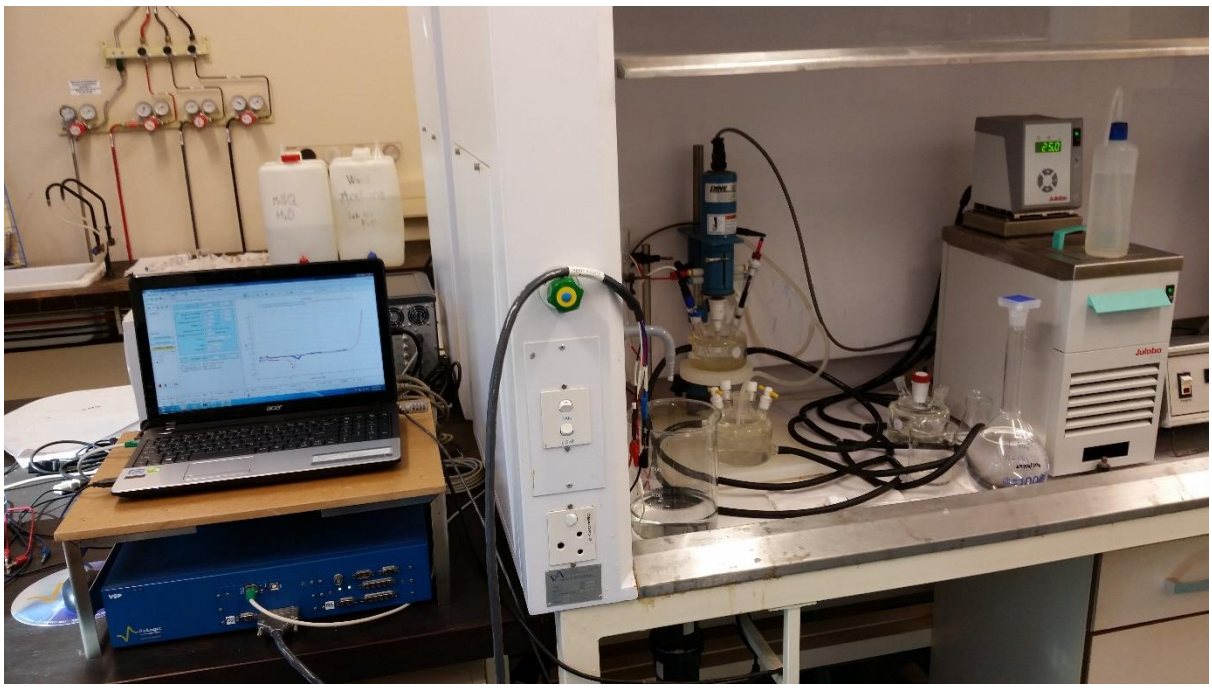

Figure 3.3: Electrochemical setup used for preconditioning, SO_2 oxidation and preliminary (acid) stability experiments

3.4.2 Stability

While the preliminary stability experiments (3.5.4. *Acid stability*) employed the exact same setup as mentioned above, the main stability experiments (3.5.4. *SO_2 oxidation stability*) required some modifications to the experimental setup. It was identical to the abovementioned setup, with the exception of the electrochemical cell, which was modified by adding an overflow. The overflow was connected to a sealed, temperature-controlled reservoir (500 mL), kept at the same temperature as the cell (25.0 °C). A glass diffuser (for bubbling SO_2 gas) and two outlets were also present on the reservoir. One outlet was connected to a SO_2 scrubber while the other was connected to a peristaltic pump (MasterFlex Console Drive). The pump was in turn connected to the electrochemical cell, forming a closed loop between the reservoir and cell. This enabled the

transfer of freshly saturated solution to the cell, with an equal amount of solution flowing out through the overflow back to the reservoir. The reason for this system (shown in Figure 3.4) is to keep the reactant (dissolved SO_2) concentration constant, which is essential due to the duration of these experiments and considering that the equilibrium potential (E_e) is influenced by the reactant and product concentrations (Nernst Equation). The simplest method is to constantly bubble SO_2 gas through the H_2SO_4 solution to keep it saturated. However, the gas cannot be bubbled in the cell due to interference with the WE and reference electrode, necessitating the use of an external vessel.

Ideally, the solution that exits the cell via the overflow should be disposed of, since H_2SO_4 is a product of SO_2 electro-oxidation. The quantity of solution required (and waste generated) per experiment, unpractical and costly for a lab-scale setup, prevented the implementation of this method.

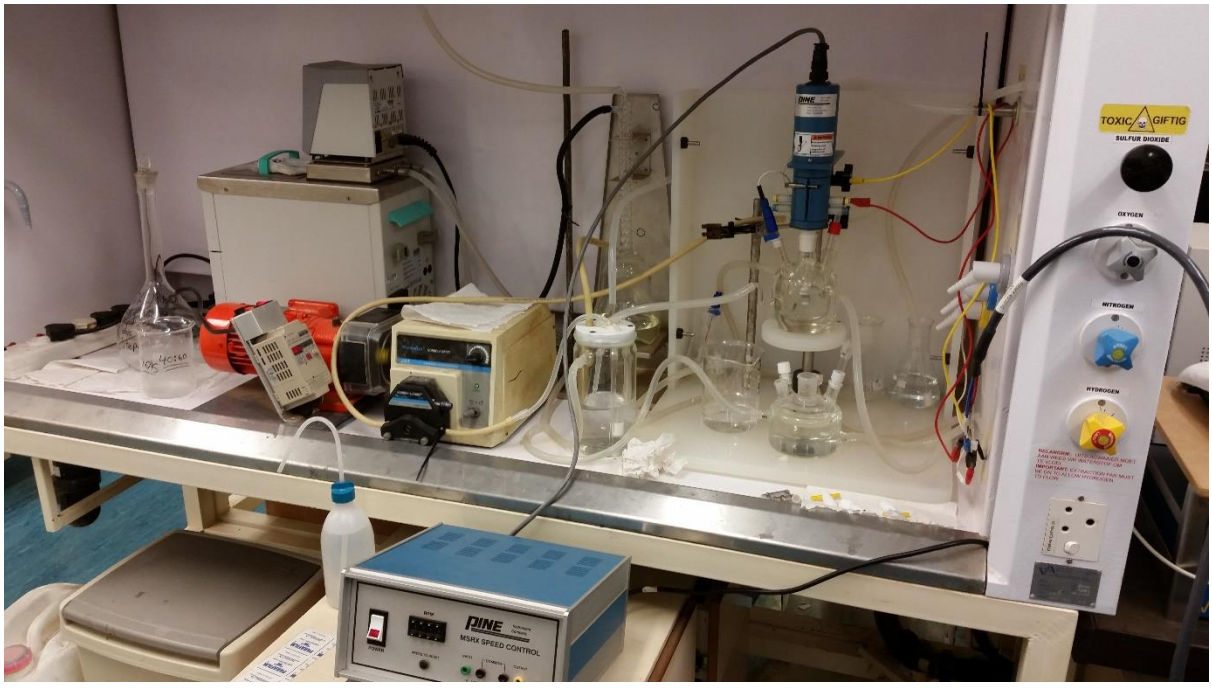

Figure 3.4: Electrochemical setup used for main (SO_2 oxidation) stability experiments

3.5 Electrochemical experiments

3.5.1 Electrolyte preparation

Before preparing the electrolyte solutions required for the experiments (1 M H_2SO_4 and 0.1 M $HClO_4$), the stock solutions were standardised to achieve the best possible correlation between experimental and theoretical parameters. Both stock solutions (95-99% H_2SO_4 and 70% $HClO_4$,

Merck) were standardised with a 1 M NaOH (Promark Chemicals; purity > 99.0%) solution, which itself was standardised with 1.000 g Potassium Hydrogen Phthalate (ACE Chemicals; purity > 99.5%). The salt, which is hygroscopic, was dried at 60 °C for 24 hours prior to the standardisation process. To ensure optimal accuracy and repeatability, a digital pipette (Eppendorf Multipette Stream) was employed in the preparation of solutions and the transfer of solutions to the cells.

3.5.2 Preconditioning procedure

All electrodes were subjected to preconditioning before being transferred to another cell for the actual experiment. Preconditioning was performed in 100 mL of 0.1 M $HClO_4$ solution, which was purged with N_2 for 15 minutes before the electrode was cycled between upper and lower potential points at specified rates. The preconditioning consisted of three different cyclovoltammogram (CV) techniques, which were run consecutively (shown in Table 3.3).

Table 3.3: Preconditioning procedure

CV technique no.	E_{Low} (V)	E_{High} (V)	dE/dt ($mV.s^{-1}$)	Cycles
1	0.041	1.441	50	25
2	0.041	1.741	50	3
3	0.041	1.441	50	3

3.5.3 SO_2 oxidation

Linear Sweep Voltammetry (LSV), also known as Linear Polarisation (LP), was used to determine the catalysts' activity towards SO_2 oxidation. The experiments were performed in a 1 M H_2SO_4 electrolyte solution, also purged with N_2 for 15 min, and SO_2 was produced *in situ* by the addition of a 1 M Na_2SO_3 (ACE Chemicals; purity > 97.0%) solution. After preconditioning the electrodes were rinsed with deionised H_2O and transferred to a cell containing 90 mL of the H_2SO_4 solution (purged with N_2 for 15 min). With the electrode wires connected and the technique loaded in the program, 10 mL of the Na_2SO_3 solution was added with a pipette to produce 100 mM SO_2. The solution was stirred immediately following this addition by rotating the WE for 5 seconds at 2500 rpm, after which the LP was initiated. The parameters employed in the LP scan are as follows: E_{Low} = 0.200 V, E_{High} = 1.441 V, dE/dt = 10 $mV.s^{-1}$.

For the Rotating Disk Electrode (RDE) experiments, the procedure followed was identical to the one used for the stationary electrodes except that the rotator was switched to a certain rotation

rate after stirring, instead of being disabled (0 rpm). Six rotation rates were included in the initial experiments (100, 200, 400, 800, 1500, 2500 rpm), of which five were used for data analysis.

3.5.4 Stability

Acid stability

In order to facilitate the large amount of catalyst samples in the first stage of the study, stability was initially assessed by potential cycling (CV) in an acidic electrolyte (100 mL 1 M H_2SO_4, purged with N_2 for 15 min) in the absence of an active species (SO_2). The potential was cycled between 0.041 V (E_{Low}) and 1.441 V (E_{High}) at a rate of 100 $mV.s^{-1}$ (dE/dt) for 200 cycles at a time. The goal of this setup is to continuously run the CV experiment until a physical disruption of the catalyst layer or a sudden drop in the amplitude of the cyclovoltammogram is observed. Between each CV experiment (200 cycles) the electrode was rotated for 5 seconds at 2500 rpm and the catalyst layer inspected; if no visual cues of instability was observed the electrode was subjected to another round of CVs.

SO_2 oxidation stability

Chronoamperometry (CA) was employed to evaluate the stability of the catalysts under working load, i.e. a constant potential (E_{Hold}) was applied, resulting in the oxidation of the active species (SO_2). After transferring 400 mL 1 M H_2SO_4 to the reservoir and sealing all contact points (lid, inlet and outlets) with Parafilm, SO_2 gas (Afrox; purity > 99.9%) was bubbled in the reservoir for at least 20 min to ensure saturation. Following this period the gas supply was slightly reduced and the peristaltic pump switched on, transferring freshly saturated solution to the cell at a rate of 20 $mL.min^{-1}$. When the solution began to overflow, the rotator was switched on to 800 rpm and the experiment could be initiated. The rotation was required due to the fact that gas bubbles formed on a stationary electrode's surface, interfering with the measurements. Considering the influence of sulphur coverage on SO_2 oxidation activity, a LP scan (E_{Low} = 0.200 V, E_{High} = 0.650 V, dE/dt = 10 $mV.s^{-1}$) was performed prior to the CA step (E_{Hold} = 0.650 V, t = 6 h), with the LP's upper potential being equal to the holding potential employed in the CA ($E_{High} = E_{Hold}$). Owing to the risk associated with SO_2, a portable gas meter was placed next to the fume hood containing the setup.

4 RESULTS & DISCUSSION

4.1 Stationary electrode experiments

4.1.1 Catalyst screening

The CVs (five cycles) of a Pt catalyst in 0.1 M $HClO_4$ can be seen in Figure 4.1, which displays the 'activation' of the catalyst surface as a result of preconditioning. The figure clearly shows that the sizes of the peaks increase with consecutive cycles, stabilising after approximately 15 cycles. For Pt, four peaks (corresponding to two processes) can be expected in the potential region employed for preconditioning, hydrogen adsorption/desorption (a nonfaradaic process) and surface oxidation/reduction. Besides an increase in the areas under the peaks, the hydrogen adsorption/desorption area displays multiple peaks after several cycles, an indication of the polycrystallinity of the Pt catalyst. Since SO_2 oxidation was being studied on an elemental metal surface, the final cycle in the preconditioning procedure was set to terminate at open cell potential (~0.550 V) during the forward scan to ensure an oxide-free surface.

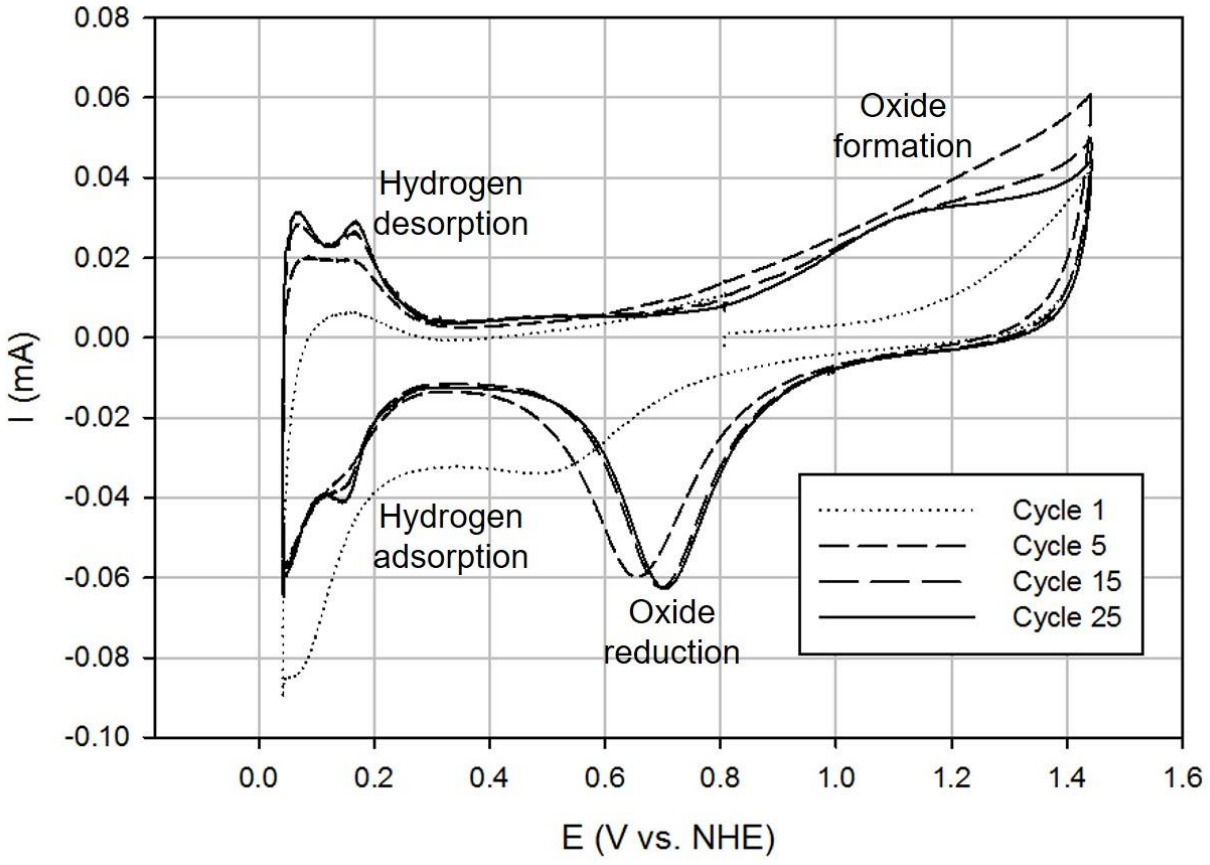

Figure 4.1: Preconditioning CVs of Pt in 0.1 M $HClO_4$ (scan rate = 50 mV.s^{-1})

While the CVs of Pd exhibit a similar profile to Pt, it is important to note that hydrogen absorbs on Pd, as opposed to adsorption on Pt. The CVs (final cycle, 0.1 M $HClO_4$) of the six initial catalysts are shown in Figure 4.2, and it can be seen that the binary catalysts exhibit peaks different from their constituent elements. It is interesting to note that the three compositions with the lowest Pt content (Pt_2Pd_3, Pt_1Pd_4 and Pt_1Pd_9) display rounded hydrogen adsorption/desorption peaks and Pd-like oxide reduction peaks, while Pt_3Pd_2 is almost identical to Pt.

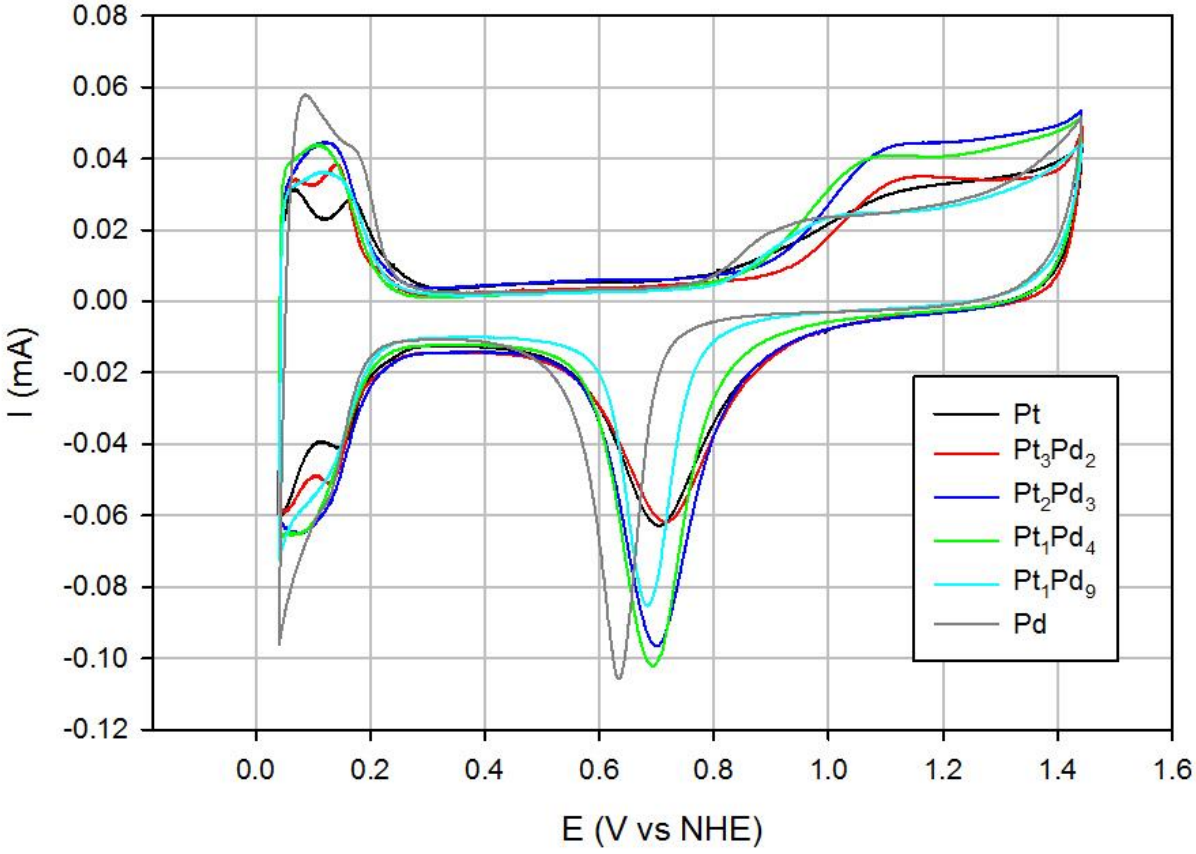

Figure 4.2: Preconditioning CVs of catalysts in 0.1 M $HClO_4$ (cycle 25, scan rate = 50 $mV.s^{-1}$)

While the CVs show that preconditioning did indeed cause a significant change in the electrochemical characteristics of the catalysts, it did not induce any observable visual changes on the macroscopic level in the electrode surfaces. Electrodes were visually inspected to confirm the physical integrity of the catalyst layers prior to being transferred to the SO_2 oxidation cell; however, none of the samples showed any signs of layer disintegration at this stage. Visual inspection was performed again upon completion of the SO_2 oxidation experiments. An example of the LP curves obtained for the catalysts is shown in Figure 4.3, with the results given in Table 4.1. At least four LPs were obtained for each catalyst, of which three were used for the determination of the activity parameters (E_i, E_p, i_p).

Table 4.1: Activity parameters of catalysts in stationary electrode experiments

Composition	Peak current density		Peak potential		Onset Potential	
	i_p (mA.cm^{-2})		E_p (V)		E_i (V)	
	Value	Std. Dev.	Value	Std. Dev.	Value	Std. Dev.
Pt	17.471	1.325	0.762	0.011	0.601	0.002
Pt_3Pd_2	19.327	0.954	0.735	0.009	0.601	0.004
Pt_2Pd_3	18.645	2.649	0.738	0.011	0.605	0.006
Pt_1Pd_4	19.986	0.74	0.745	0.011	0.616	0.007
Pt_1Pd_9	15.23	2.267	0.774	0.004	0.635	0.002
Pd	17.255	0.925	0.771	0.008	0.659	0.005

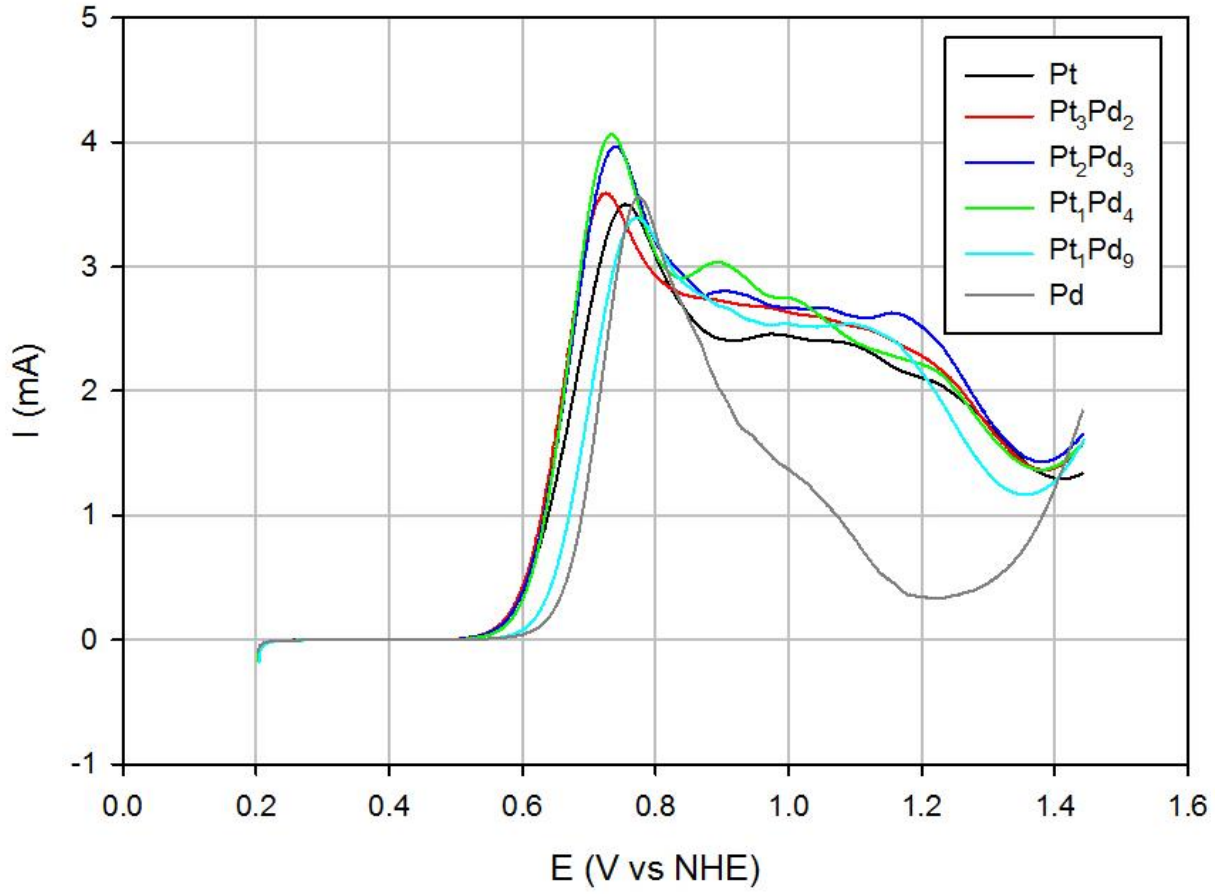

Figure 4.3: SO_2 oxidation LP curves of catalysts in 1 M H_2SO_4 + 100 mM SO_2 (stationary electrode, scan rate = 10 mV.s^{-1})

As can be seen in Figure 4.3, the binary compositions exhibit LP curves similar to Pt in the respect that a sort of plateau is achieved before the current significantly drops. The position and size of the first peak, however, vary between the catalysts. Due to the fact that the electrode is stationary during SO_2 oxidation, a drop in current can be expected as a result of mass-transport effects. The sudden current drop observed at ~1.200 V for Pt can however be attributed to the 'deactivation' of the catalyst. This is a result of the blockage of active sites on the surface by surface oxides, which exert an inhibitory effect on SO_2 oxidation activity [3]. Although surface oxidation begins at ~0.800 V, significant oxidation only occurs at potentials above ~1.200 V, as can be seen in Figure 4.1 and Figure 4.2. A noticeable difference between the LP curves of Pt (as well as the binary catalysts) and Pd is the rapid current decay observed for the Pd electrodes (Figure 4.3). This rapid drop in current can be explained by referring to Figure 4.2, which shows that while Pd surface oxidation also commences at ~0.800 V, significant oxidation occurs at potentials above ~1.000 V. It is interesting to note that although Pd is 'deactivated' to a significantly greater degree than Pt as the potential is increased, none of the binary catalysts display this significant deactivation. The LP curves of the binary composition with the highest Pd content (Pt_1Pd_9) are very similar to those of Pt with respect to the behaviour observed at potentials above ~0.900 V (Figure 4.3).

As mentioned above, a visual inspection of the catalyst layer was performed upon completion of the LP experiments. Layer disintegration could be observed for approximately half of the Pt_1Pd_4 electrodes, and for all the Pt_1Pd_9 and Pd electrodes. In all cases the layer disintegrated when the electrodes were rinsed with H_2O after removal from the cell. No signs of layer disintegration could be observed on any electrodes of the other catalysts. In this study, layer disintegration is defined as the separation of a fragment of the catalyst layer from the GC support. An example of an electrode with a disintegrated catalyst layer is shown in Figure 4.4. Obtaining three successful LP curves of Pt_1Pd_9 and Pd also proved to be difficult, owing to the fact that layer disintegration occurred prior to the initiation of the LP experiment in more than half of these electrodes. In all cases the layers disintegrated when the electrode was rotated for 5 seconds at 2500 rpm. The formation of SO_2 bubbles on the WE surface after the injection of Na_2SO_3 solution into the cell necessitated the rotation of the electrode prior to the initiation of the LP experiment. In the cases noted above fragments of catalyst layer could be visually observed in the solution when the rotator was engaged. When the timing of the disintegration is considered, the assumption can be made that the force exerted on the electrode surface by convection of the solution caused the layer to break apart. The cause of the underlying 'instability' in the Pt_1Pd_9 and Pd catalyst layers that resulted in fragmentation is however unclear. Two possible causes for the instability in Pd-rich layers are considered: the layer was physically unstable (i.e. Pd does not adhere to a GC support as well as Pt) or chemically unstable (i.e. Pd dissolves in a 1 M H_2SO_4 solution). Additional data (e.g. ICP-MS) is required for a definite conclusion. However this is beyond the scope of this study.

Figure 4.4: Electrode with disintegrated catalyst layer

Apart from the instability observed for the Pd-rich compositions, all catalysts were found to be active towards SO_2 oxidation. The activity parameters given in Table 4.1 were determined with the method shown in Figure 2.3. E_p and I_p were taken as the coordinates of the first peak, while E_i was taken as the intercept of two tangents [34]. Although all three parameters are arguably equally important, caution should be exercised when comparing the i_p values. The geometric area of the electrodes (0.196 cm^2) was used to calculate the current density, which results in a certain degree of uncertainty due to the fact that the electrochemically active surface area (ECSA) is usually vastly greater than the planar geometric area. The ECSA represents the 'true catalytically active surface area', as the surface is not planar on a microscopic level, and it can be calculated with several electrochemical methods (e.g. hydrogen adsorption/desorption and underpotential deposition of a metal). Choice of method is determined by the composition of the electrode, with an applicable method available for most pure metal electrocatalysts. When the catalyst consists of more than one metal, the ECSA can only be determined if a method is applicable to all the constituent elements. Furthermore, the optimal parameters employed in a specific method (e.g. holding potential) for ECSA determination are unique for each metal. As a result, successful determination of ECSA in binary and ternary catalysts usually requires extensive method optimisation. Apart from method optimisation, many of these techniques require multiple experiments and a fair amount of data analysis, and it is thus not surprising that geometric area is employed in the majority of electrocatalysis studies.

By comparing the results of Pt and Pd (Table 4.1), it is evident that Pt is more active towards SO_2 electro-oxidation than Pd. While these catalysts display similar peak current densities, Pt exhibits lower onset and peak potentials. Considering the instability, as well as the slightly decreased catalytic activity observed for the Pd electrodes, it can be concluded that Pt is more suitable as catalyst material for SO_2 electro-oxidation than Pd. Owing to the instability of the Pt_1Pd_9 electrodes, this catalyst can also be eliminated as a possible replacement for Pt, regardless of its activity. This leaves three binary catalysts (Pt_3Pd_2, Pt_2Pd_3 and Pt_1Pd_4) that can be compared to Pt, of which one will be chosen for further study alongside Pt. In terms of peak current, comparison between these values is difficult due to the relatively large standard deviation of the Pt and Pt_2Pd_3 catalysts. Taking this into account, some conclusions can still be made. Both Pt_3Pd_2 and Pt_1Pd_4 display higher peak current densities (19.327 $mA.cm^{-2}$ and 19.986 $mA.cm^{-2}$, respectively) than Pt (17.471 $mA.cm^{-2}$), with Pt_1Pd_4 displaying the highest peak current density overall. Although the peak current density of Pt_2Pd_3 (18.645 $mA.cm^{-2}$) is higher than that of Pt, the standard deviation of this value is 2.649, making a definite conclusion impossible. In general, the three binary compositions display peak current densities higher or similar to Pt, suggesting that incorporation of these amounts of Pd into Pt possibly results in improved electrode kinetics. Due to the uncertainty caused by the standard deviation of some of these values and the issue of geometric area, a definite conclusion is not possible.

In the analysis of the activity parameters, the approximation was made that the peak current densities of Pt and the three binary catalysts were equal, and thus only the onset and peak potentials (E_i and E_p, respectively) were considered in the determination of the binary composition to be studied further. In terms of onset potential, Pt and Pt_3Pd_2 exhibited the lowest values (0.601 V for both), with Pt_2Pd_3 and Pt_1Pd_4 displaying slightly higher onset potentials (0.605 V and 0.616 V, respectively). If the standard deviation of these values is considered, it can be concluded that Pt, Pt_3Pd_2 and Pt_2Pd_3 are identical with respect to onset potential. It is interesting to note that while Pd displayed the highest onset potential (0.659 V), the addition of Pd to a Pt catalyst did not result in significantly higher onset potentials (even with only 20% Pt content, as in Pt_1Pd_4). Comparing the peak potentials also revealed a noteworthy occurrence: the three binary catalysts all displayed lower peak potentials than both Pt and Pd. Although the peak potential was slightly lower for Pt than Pd (0.762 V vs. 0.771 V), the peak potentials for these two catalysts were assumed to be equal due to the standard deviation of these values. Pt_3Pd_2 displayed the lowest peak potential (0.735 V), with Pt_1Pd_4 exhibiting the highest peak potential (0.745 V) of the three binary catalysts. The peak potential for Pt_2Pd_3 was only marginally higher than Pt_3Pd_2 (0.738 V vs. 0.735 V), however the peak potential of these two catalysts were approximated to be equal, again due to the standard deviation. While the standard deviation of the peak potentials makes a clear distinction between the three binary catalysts difficult, it is evident from the results in Table 4.1 that these catalysts exhibit lower peak potentials than both their constituent elements. This

indicates that the combination of these two elements in certain ratios possibly results in an electrocatalyst with more favourable catalytic properties than either Pt or Pd. Whether this is due to improved thermodynamics remains unclear; both Pt_3Pd_2 and Pt_2Pd_3 exhibit reduced peak potentials compared to Pt, but with similar onset potentials.

Regarding the binary catalyst to be used in further experiments, both Pt_3Pd_2 and Pt_2Pd_3 stand out as viable candidates. Although these two binary catalysts exhibit similar activity parameters, Pt_3Pd_2 appears to be the composition with the highest catalytic activity (if the values are taken as absolute). Apart from the activity, concerns about catalyst layer stability during RDE experiments (constant rotation) merited the use of the composition with the lowest Pd content. Thus, Pt_3Pd_2 was chosen for further study alongside Pt.

4.1.2 Annealing temperature screening

Surface characterisation

SEM/EDX was performed on four electrodes of both Pt and Pt_3Pd_2 to confirm the compositions and get a visual indication of any differences on the electrode surfaces induced by the annealing process. The electrodes were submitted for analysis after sputtering, and again after the same electrodes had been annealed, one at each annealing temperature (No. 1: 600 °C, No. 2: 700 °C, etc.). The EDX results of the initial analysis are given in Table 4.2, with the results of the second analysis shown in Table 4.3.

Table 4.2: EDX results (atomic %) of non-annealed Pt and Pt_3Pd_2 catalysts

Pt		**No.**	**Pt_3Pd_2**	
Pt	Pd		Pt	Pd
100	0	**1**	55.49	44.51
100	0	**2**	59.33	40.67
100	0	**3**	63.58	36.42
100	0	**4**	63.74	36.26
100	0	**Average**	60.54	39.46
0.00		**Std. Dev.**	3.93	

Table 4.3: EDX results (atomic %) of annealed Pt and Pt_3Pd_2 catalysts

Pt		Temperature	Pt_3Pd_2	
Pt	Pd		Pt	Pd
100	0	**600 °C**	55.79	44.21
100	0	**700 °C**	57.35	42.65
100	0	**800 °C**	65.79	34.21
100	0	**900 °C**	62.67	37.33
100	0	**Average**	60.40	39.60
0.00		**Std. Dev.**	4.65	

The initial analysis (Table 4.2) reveals that there is a small variation in the composition of the four Pt_3Pd_2 electrodes, although the average composition is approximately equal to the theoretical composition. All the Pt electrodes contained 100% Pt, with identical results obtained after annealing (Table 4.3). The variation in the composition of the Pt_3Pd_2 electrodes is most likely a result of the placement of the electrodes in the sputtering tray. Because each metal is contained in a different magnetron, some slots in the sputtering tray are closer to the Pt source than the Pd source (and vice versa). Another possible explanation for this variation is that the distribution of the two metals on the surface is different on each electrode. Although the total composition would be 60% Pt : 40% Pd on all the electrodes, the EDX results can still differ since only a fraction of the total electrode surface is scanned. In order to draw a definite conclusion, additional experimentation with electrode placement in the sputtering tray, as well as SEM/EDX analysis, is required. By comparing the results of the non-annealed electrodes of Pt_3Pd_2 with their annealed counterparts (Table 4.3), it can be seen that composition varies slightly. The largest variations were observed for 700 °C and 800 °C (~2%), while the difference for 600 °C is negligible. It is however very unlikely that the total atomic ratio of the catalyst layer is influenced by the annealing process, seeing that the highest annealing temperature (900 °C) is well below the melting points of both Pt and Pd. Thus, while the annealing process can induce the migration of atoms in the layer (which in turn influences crystallinity and surface morphology), the total number of Pt and Pd atoms in the layer remains constant. If the atoms migrate within the layer but only a fraction of the area is scanned, it is logical that the EDX results would differ. It is important to note that, due to the thinness of the catalyst layers (60 nm), the data obtained in the EDX analysis is acquired from the entire catalyst layer and not just the surface layer of atoms.

The images obtained with SEM confirm that annealing does indeed cause a change in the surface morphology of both Pt and Pt_3Pd_2 catalyst layers. The micrographs of the two non-annealed catalysts are nearly indistinguishable from one another, appearing only as a haze of fine dots. A clear trend could be observed for both catalysts, as the SEM micrographs of Pt_3Pd_2 show in Figure 4.5. An increase in T_{High} results in increased grain growth and better defined grain boundaries, with the lowest temperature (600 °C) displaying approximately identical grain sizes as the non-annealed catalysts, but with clearly defined boundaries.

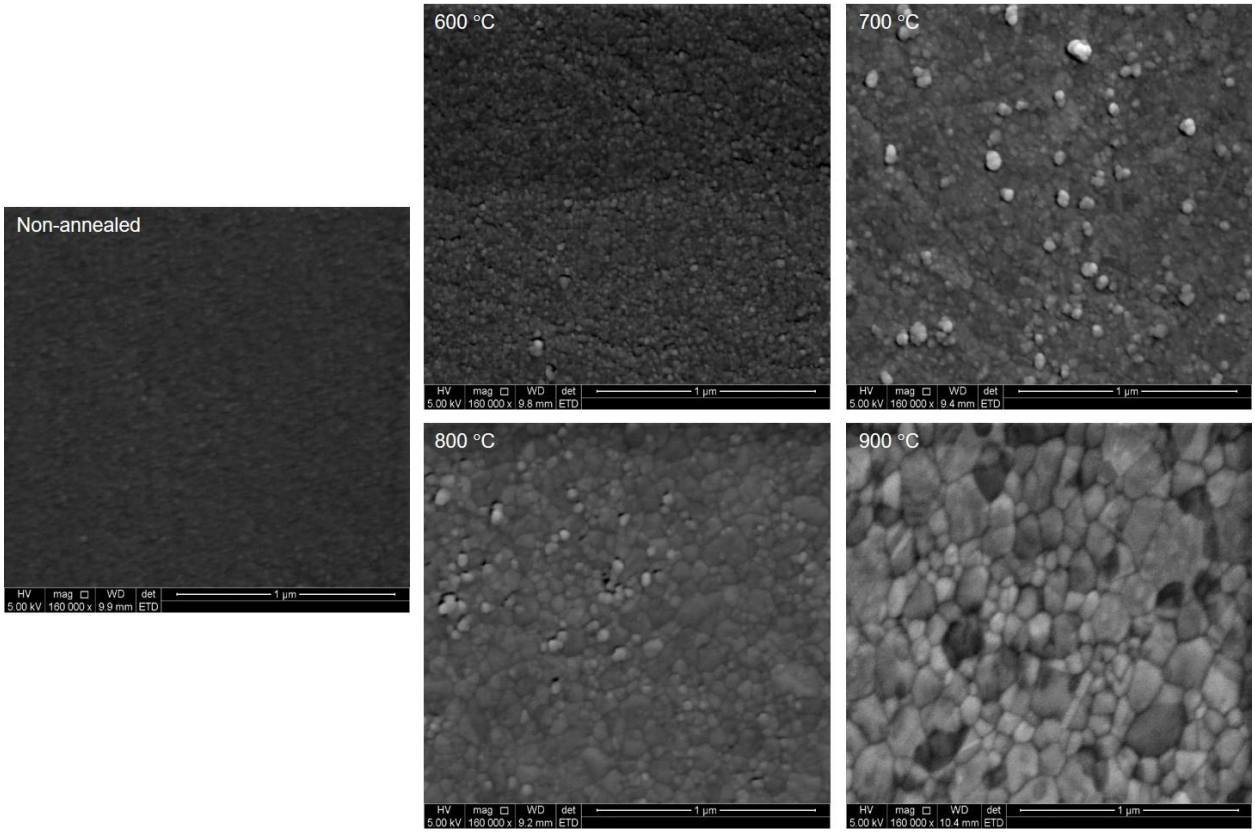

Figure 4.5: SEM micrographs of non-annealed and annealed Pt_3Pd_2 catalysts

Although no quantitative data about the electrode surfaces could be obtained with SEM/EDS, AFM analysis of the catalysts provided both two and three dimensional (2D and 3D) topographical maps of the surfaces as well as quantitative data. While the AFM images provide valuable qualitative data on the effect of annealing temperature on the surface topography, a meaningful comparison between the catalysts is only possible with the various surface parameters determined in the analysis. The 2D images of non-annealed and annealed Pt_3Pd_2 are shown in Figure 4.6, while the 3D images of both Pt and Pt_3Pd_2 (non-annealed and annealed) can be found in Figure 4.7. AFM analysis produces multiple parameters related to surface topography; the main parameters employed to describe surface roughness are the average and root mean square

(RMS) roughness (R_a and R_q, respectively) [35]. The average roughness is defined as the arithmetic average deviation in surface height from the mean plane, while RMS roughness is defined as the root mean square average of height deviations from the mean plane [36].

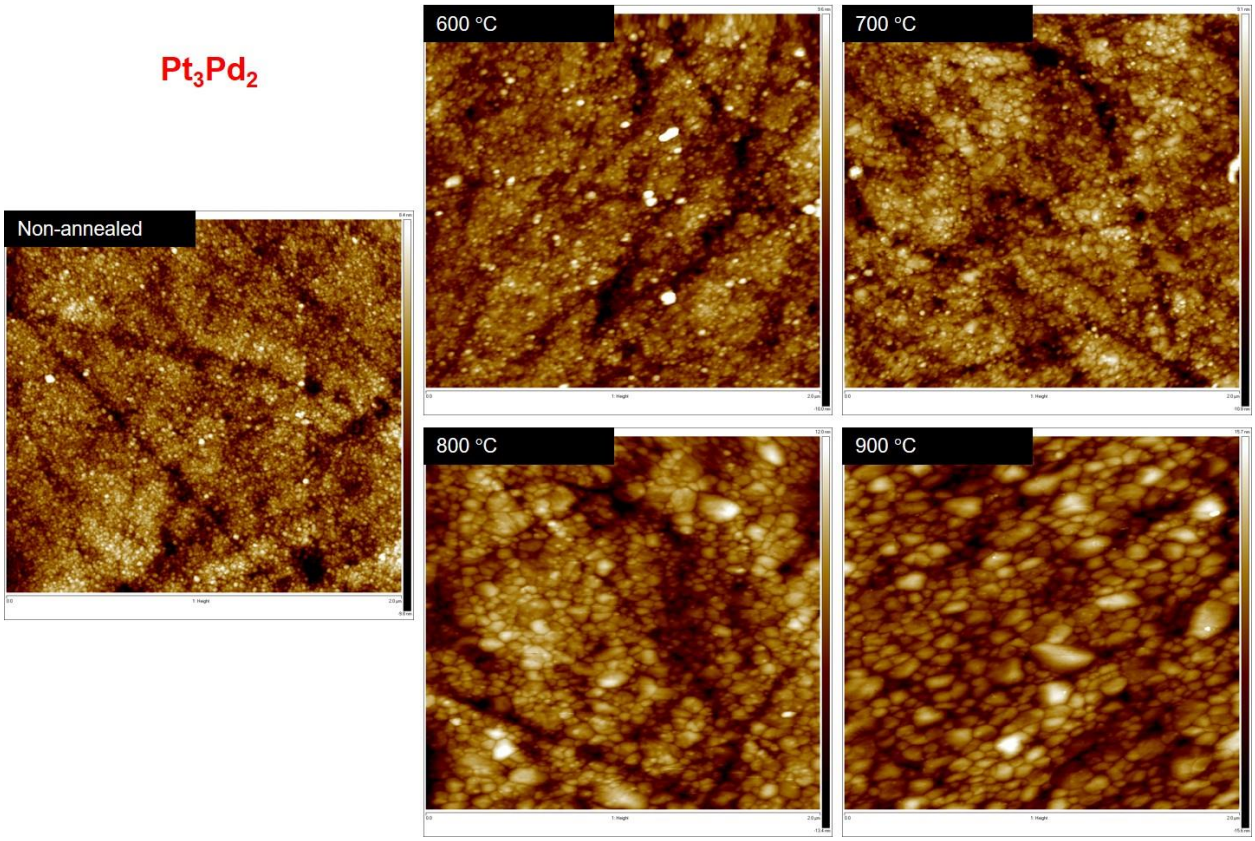

Figure 4.6: 2D AFM images of non-annealed and annealed Pt_3Pd_2 catalysts

The average and RMS roughness values of the Pt and Pt_3Pd_2 (non-annealed and annealed) catalysts obtained from AFM analysis are shown in Table 4.4. Comparison of the roughness parameters to the 3D images in Figure 4.7 reveals that the 3D topographical maps are good visual representations of the quantitative data.

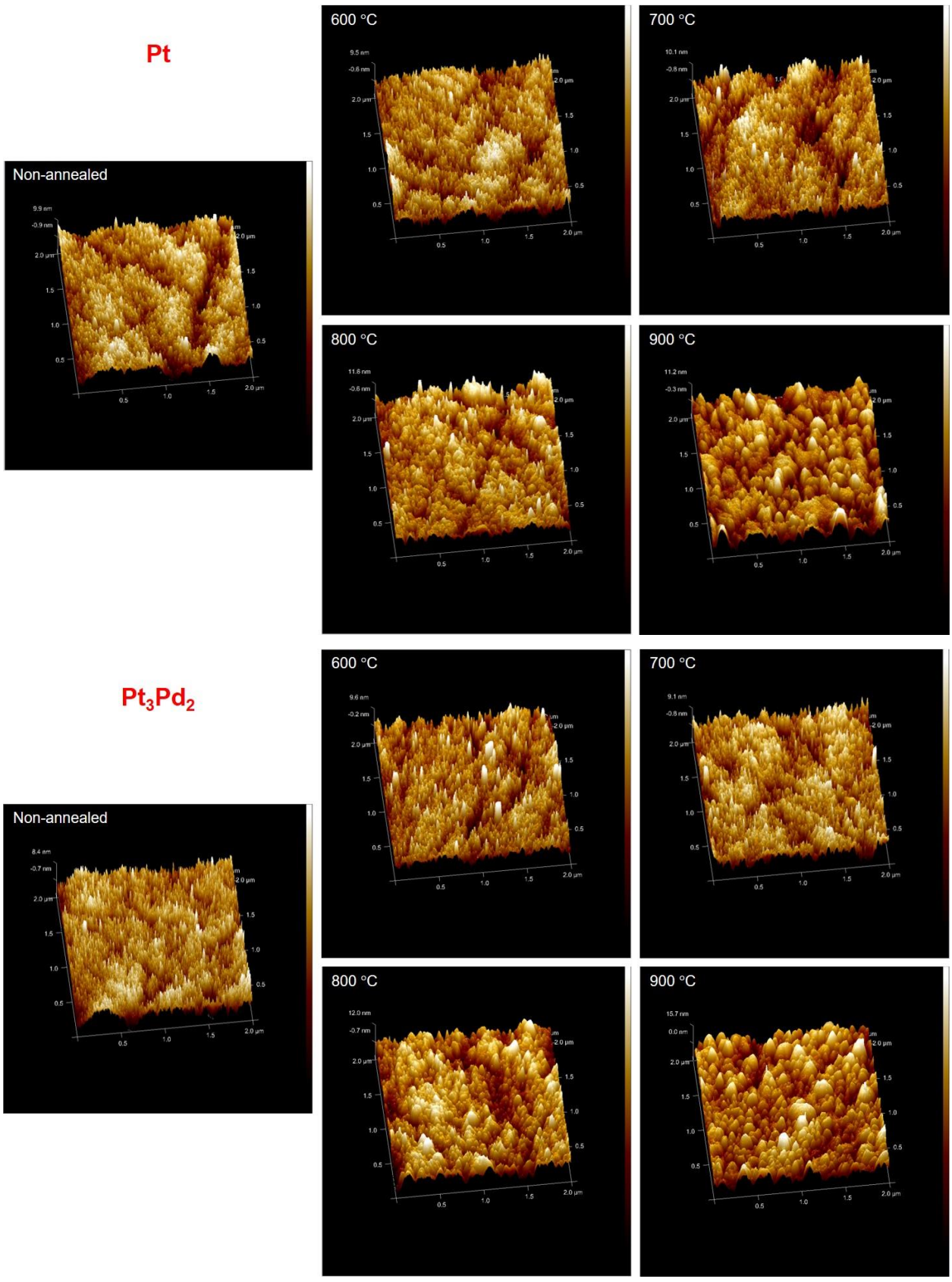

Figure 4.7: 3D AFM images of non-annealed and annealed Pt (top) and Pt_3Pd_2 (bottom) catalysts

Table 4.4: Surface roughness parameters of non-annealed (NA) and annealed Pt and Pt_3Pd_2 catalysts

Pt		Temperature	Pt_3Pd_2	
R_a	R_q		R_a	R_q
2.43	3.11	**NA**	1.83	2.38
2.27	2.90	**600 °C**	1.99	2.65
2.19	2.86	**700 °C**	2.25	2.94
2.49	3.26	**800 °C**	2.71	3.44
2.49	3.22	**900 °C**	3.40	4.38

Of the two non-annealed catalysts, Pt displays the highest roughness parameters. An increase in T_{High} up to 700 °C results in a small decrease in these values, while 800 °C and 900 °C display nearly identical values, slightly higher than non-annealed Pt. A different trend is observed for the annealed Pt_3Pd_2 catalysts, where the lowest annealing temperature (600 °C) displays higher values than the non-annealed catalyst, and the values increase with increasing T_{High} over the entire temperature range. The roughness parameters in Table 4.2 also reveal that annealing (at the T_{High} points studied) has a more pronounced effect on R_a and R_q values of the Pt_3Pd_2 catalyst surfaces in comparison to Pt, and at temperatures of 700 °C and above the roughness parameters of Pt_3Pd_2 exceed those of Pt. The range of these values is thus also significantly larger for Pt_3Pd_2 than Pt (ΔR_a = 0.30 nm and ΔR_q = 0.40 nm for Pt vs. ΔR_a = 1.57 nm and ΔR_q = 2.00 nm for Pt_3Pd_2). Since AFM was only performed on a single binary composition, the exact role of Pd in this occurrence remains unclear. Although Pd might inherently be more influenced by annealing than Pt, it is also possible that the increased effect is a result of altered electronic properties in the binary Pt_3Pd_2 catalyst layer due to electronic interaction between the Pt and Pd atoms.

Although higher roughness parameters are favourable since they imply a larger 3D geometric area, the ECSA does not necessarily increase to the same extent as the geometric area. ECSA is not only influenced by the geometric area, but also by specific surface features, such as the number of active centres and the electronic properties of the surface layer atoms (both of which are dependent on the location and identity of the surface and subsurface atom layers). While a correlation between roughness parameters and ECSA for a pure metal catalyst can possibly be determined with enough data from electrochemical experiments and AFM, as well as XRD analysis, it would be a very complex and time-consuming process.

XRD analysis revealed that the annealing process also has an effect on the crystallinity and crystallite size of both Pt and Pt_3Pd_2. The non-annealed catalyst layers were found to be mainly amorphous in nature, in accordance with the lack of clear grain boundaries observed in the SEM images of the two catalysts. As with SEM/EDX, the data obtained with XRD also applies to the entire catalyst layer. The X-rays generated by the diffractometer seemingly penetrate to depths well below the 60 nm catalyst layer into the GC support, with the Pt and Pd peaks barely visible above the background noise in the diffractograms of the non-annealed catalysts. In fact, XRD analysis on catalyst layers 40 nm thick fails to detect either Pt or Pd, with results indicating that only carbon was present.

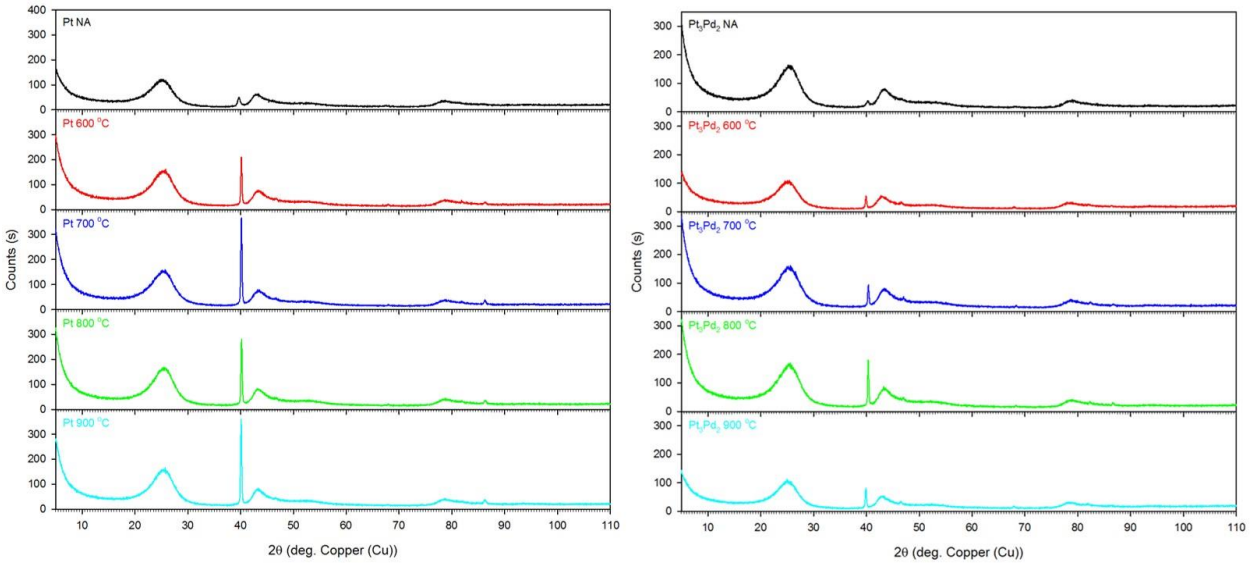

Figure 4.8: Diffractograms of non-annealed (NA) and annealed Pt and Pt_3Pd_2 catalysts

The diffractograms of the Pt and Pt_3Pd_2 catalysts are shown in Figure 4.8, with the crystallite sizes given in Table 4.5. The three broad peaks present in all diffractograms were attributed to carbon, with the diffractograms of both non-annealed catalysts displaying only a single additional peak (2θ = ~40°), corresponding to the (111) crystal plane of the face-centered cubic (FCC) metals. Although the peaks are not visible on the diffractograms, the data indicates the presence of multiple crystal planes, implying that the catalyst layers are polycrystalline. Upon close inspection some of these peaks are however visible on the diffractograms of the annealed Pt and Pt_3Pd_2 catalysts. Furthermore, the annealed catalysts also exhibit an increase in the intensity of the peak corresponding to the (111) crystal plane, indicating that annealing causes an increase in the degree of crystallinity of both Pt and Pt_3Pd_2 catalyst layers. The increase in the peak intensity is more pronounced on the annealed Pt catalysts than on their Pt_3Pd_2 counterparts, with all the annealing temperatures displaying a significantly sharper peak than non-annealed Pt. Annealing

at 700 °C and 900 °C resulted in the highest intensity, followed by annealing at 800 °C. Although the diffractograms of the annealed Pt_3Pd_2 catalysts are readily distinguishable from their non-annealed counterpart, only annealing at 800 °C resulted in a significant increase in peak intensity. These observations are also reflected by the crystallite sizes (Table 4.5), with 900 °C exhibiting the largest crystallites for Pt while 800 °C displayed the largest crystallite size for Pt_3Pd_2.

Table 4.5: Crystallite sizes of non-annealed (NA) and annealed Pt and Pt_3Pd_2 catalysts

Pt	**Temperature**	**Pt_3Pd_2**
Crystallite size (Å)		**Crystallite size (Å)**
180	**NA**	212
564	**600 °C**	497
564	**700 °C**	564
564	**800 °C**	605
604	**900 °C**	528

SO_2 oxidation

The preconditioning CVs and SO_2 oxidation LPs of the annealed Pt and Pt_3Pd_2 catalysts are shown in Figure 4.9 and Figure 4.10, respectively, with a CV/LP of each non-annealed catalyst included for visual comparison. It is immediately evident from the LP curves (as well as the CVs) that annealing at any temperature has a pronounced effect on the electrochemical behaviour of both Pt and Pt_3Pd_2. The influence of the annealing temperature on the size and shape of the LPs is however different for the two compositions, with neither displaying any clear trends. Upon comparison of all data sets the only noteworthy occurrences that could visually be observed is that annealing causes a decrease in activity (decrease in I_p, increases in E_p and E_i) for both Pt and Pt_3Pd_2, and that it results in smoother LP curves for Pt (less current decay after the peak current is achieved). The enhanced plateau region observed for the annealed Pt catalysts is most likely the result of the inhibition of oxide formation/reduction (visible in Figure 4.9), although the reason why it does not translate to the LPs of the annealed Pt_3Pd_2 catalysts remains unclear.

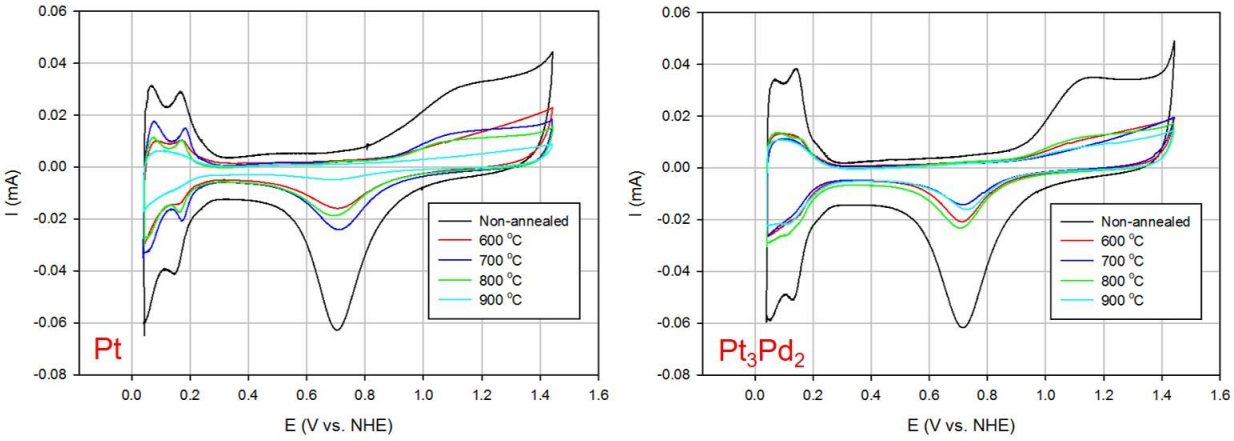

Figure 4.9: Preconditioning CVs of annealed Pt and Pt_3Pd_2 catalysts in 0.1 M $HClO_4$ (cycle 25, scan rate = 50 mV.s^{-1})

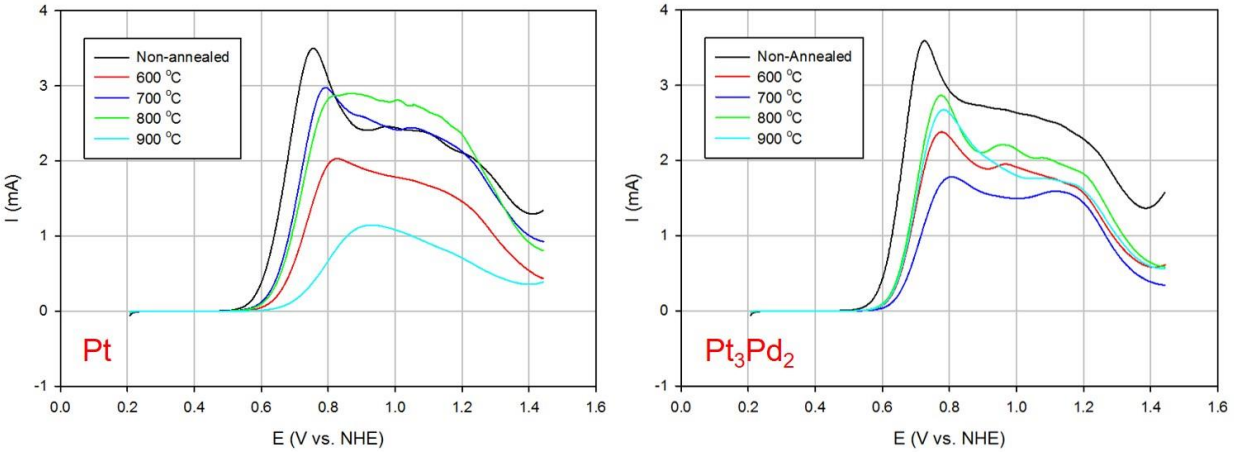

Figure 4.10: SO_2 oxidation LP curves of annealed Pt and Pt_3Pd_2 catalysts in 1 M H_2SO_4 + 100 mM SO_2 (stationary electrode, scan rate = 10 mV.s^{-1})

The activity parameters for the annealed catalysts were determined in the same manner as before, and the results of the annealed Pt catalysts can be found in Table 4.6. The values of the non-annealed catalyst are obtained from the corresponding composition in Table 4.1. The activity parameters in Table 4.6 indicates that annealing (at the T_{High} points studied) has a negative impact on the SO_2 oxidation activity of Pt. Repeatability was also an issue at some annealing temperatures (most noticeably 600 °C), as is evident from the standard deviation of some values. Nonetheless, these activity parameters still paint an interesting picture. Although annealing at all four T_{High} points resulted in decreased catalytic activity, the extent of this inhibition is most pronounced on the lowest and highest annealing temperatures (600 °C and 900 °C), with 900 °C displaying the worst activity parameters by far. Annealing at 700 °C and 800 °C displayed the

highest activities of the annealed catalysts, with 700 °C displaying slightly better values than 800 °C. Although the peak current density of 700 °C is lower than that of the non-annealed catalyst (15.694 $mA.cm^{-2}$ vs. 17.471 $mA.cm^{-2}$), the difference is small in comparison to the peak current densities of 600 °C and 900 °C (8.891 $mA.cm^{-2}$ and 5.789 $mA.cm^{-2}$, respectively). While the peak current density of 800 °C (11.090 $mA.cm^{-2}$) is lower than that of 700 °C, the large standard deviation of this value (3.212) excludes it from comparison. In terms of peak and onset potential, both 700 °C and 800 °C display nearly identical values (E_p = ~0.825 V, E_i = ~0.651 V), with potentials significantly lower than those observed for 900 °C (ΔE_p = 120 mV, ΔE_i = 50 mV). While 700 °C appears to be the best annealing temperature for Pt, it is clear from the activity parameters in Table 4.6 that both 700 °C and 800 °C exhibit the most favourable parameters of the four T_{High} points, suggesting that the optimal T_{High} point is likely between 700 – 800 °C.

Table 4.6: Activity parameters of non-annealed and annealed Pt catalysts in stationary electrode experiments

Temperature	Peak current density		Peak potential		Onset Potential	
	i_p ($mA.cm^{-2}$)		E_p (V)		E_i (V)	
	Value	Std. Dev.	Value	Std. Dev.	Value	Std. Dev.
NA	17.471	1.325	0.762	0.011	0.601	0.002
600 °C	8.891	2.434	0.874	0.052	0.669	0.024
700 °C	15.694	1.759	0.821	0.030	0.650	0.009
800 °C	11.090	3.212	0.829	0.009	0.651	0.010
900 °C	5.789	0.0555	0.942	0.013	0.704	0.011

The activity parameters of the annealed Pt_3Pd_2 catalysts are shown in Table 4.7. The values confirm the visual observation that annealing has a less pronounced negative effect on the activity of the Pt_3Pd_2 catalyst layers, although all annealing temperatures still exhibit lower activities than the non-annealed catalyst. As is the case with Pt, there is no linear correlation between temperature and activity. Interestingly, there are also two T_{High} points that stand out (again exhibiting nearly identical activity parameters), but unlike Pt these two T_{High} points are not consecutive. Another noticeable difference between the two data sets is the increase in the degree of repeatability for the annealed Pt_3Pd_2 catalysts. Annealing at 600 °C and 800 °C resulted in the highest activity, with these T_{High} points displaying approximately identical peak and onset

potentials (E_p = ~0.787 V, E_i = ~0.636 V) and 800 °C displaying the highest peak current density of the two (14.179 mA.cm^{-2} vs. 12.313 mA.cm^{-2}). Surprisingly, the annealing temperature that resulted in the highest activity for Pt produced the worst activity parameters when applied to Pt_3Pd_2, while annealing at 900 °C (worst activity for Pt) resulted in a marginally higher activity. Unlike Pt, it is unclear in what range the optimal T_{High} point for the Pt_3Pd_2 catalyst layer lies, with the optimal temperature most likely around 600 °C or 800 °C.

Table 4.7: Activity parameters of non-annealed and annealed Pt_3Pd_2 catalysts in stationary electrode experiments

Temperature	Peak current density		Peak potential		Onset Potential	
	i_p (mA.cm^{-2})		E_p (V)		E_i (V)	
	Value	Std. Dev.	Value	Std. Dev.	Value	Std. Dev.
NA	19.327	0.954	0.735	0.009	0.601	0.004
600 °C	12.313	1.757	0.787	0.019	0.634	0.005
700 °C	9.039	0.81	0.824	0.016	0.65	0.007
800 °C	14.179	0.518	0.786	0.008	0.637	0.004
900 °C	10.349	2.882	0.809	0.027	0.644	0.006

Comparing of the annealing data for Pt (Table 4.6) with that of Pt_3Pd_2 (Table 4.7) shows that there is a significant difference in the degree to which annealing inhibits the catalytic activity of the Pt and Pt_3Pd_2 catalyst layers. The difference between the activity parameters of the worst annealing temperature and the non-annealed catalyst of Pt (Δi_p = 11.682 mA.cm^{-2}, ΔE_p = 180 mV, ΔE_i = 103 mV) is relatively large when compared to Pt_3Pd_2 (Δi_p = 10.288 mA.cm^{-2}, ΔE_p = 89 mV, ΔE_i = 49 mV). In terms of the difference between the best common annealing temperature (800 °C) and the non-annealed catalyst, the smallest decrease in activity is again exhibited by Pt_3Pd_2 (Δi_p = 5.148 mA.cm^{-2}, ΔE_p = 51 mV, ΔE_i = 36 mV vs. Δi_p = 6.381 mA.cm^{-2}, ΔE_p = 67 mV, ΔE_i = 50 mV). Although the annealing of Pt at 700 °C results in marginally improved activity when compared to 800 °C, the fact that it displayed the worst activity parameters of the annealed Pt_3Pd_2 catalysts excludes it as the annealing temperature to be employed for the RDE experiments.

Furthermore, these results also indicate that there is no clear correlation between the surface roughness parameters, degree of crystallinity and crystallite sizes of the sputtered catalysts and their SO_2 oxidation activity. Thus, a change in any of these 'layer parameters' does not

necessarily result in altered SO_2 oxidation activity. This again highlights the complex nature of electrode reactions, with the electrochemical properties (such as catalytic activity) of a catalyst the product of the interplay between a multitude of surface, bulk material, and electrochemical parameters.

Acid stability

In order to assess the influence of annealing temperature on the stability of the Pt and Pt_3Pd_2 catalyst layers the electrodes were subjected to potential cycling in an acidic electrolyte (1 M H_2SO_4) in the absence of an active species (SO_2). Although information regarding layer stability under load (i.e. active SO_2 electro-oxidation) cannot be obtained with this method, it does provide an insight into the chemical stability of the layer in the electrolyte (in the potential range studied), as well as the physical stability.

As mentioned in Section 4.1.1, layer stability proved to be an issue with the Pd-rich compositions, where layer disintegration prior to SO_2 oxidation occurred in several electrodes. Two causes of the underlying instability of these catalyst layers were proposed: Pd dissolves in the 1 M H_2SO_4 electrolyte solution (chemically unstable), and/or Pd does not adhere to the GC support as strongly as Pt (physically unstable). While information regarding the latter is basically non-existent, the dissolution of Pd during potential cycling in acidic solutions has been studied. It has been conclusively shown that Pd dissolves in a H_2SO_4 electrolyte solution above certain potentials. In a 1 M H_2SO_4 solution Pd dissolution was observed at potentials above 1.0 V [37], while dissolution occurred at potentials above 0.8 V in a 0.5 M H_2SO_4 solution [38]. The authors of both papers state that Pd dissolution increases with an increase in the upper potential limit (E_{High}). One study also found that Pd dissolved in a 1 M $HClO_4$ solution, with dissolution of the bulk Pd electrode occurring at or above potentials of 0.991 V [38]. Whether or not the presence of Pt in a binary Pt_xPd_y catalyst affects the dissolution behaviour of Pd is not known; however, since the upper potential limit employed in both potential cycling and linear polarisation (E_{High} = 1.441 V) is well above the specified potentials (~1.0 V), it is assumed that Pd dissolution occurs during preconditioning (which was also included in the acid stability experiments) as well as SO_2 oxidation [39]. This is most likely the root cause of the instability observed for the Pd-rich catalyst layers. As the Pd atoms on the surface dissolve they expose the atoms directly beneath them to the electrolyte, resulting in the dissolution of Pd atoms inside the catalyst layer. The defects formed in the metal layer (e.g. cracks, pits) by this process compromise the structural integrity of the catalyst layer, which ultimately results in the physical disintegration of the layer. Although it is plausible that the decrease in structural integrity is only due to Pd dissolution, there are possibly other contributing factors. Apart from the physical stability of Pd (unknown), the structural integrity of the catalyst layer can also be influenced by hydrogen absorption. As opposed to hydrogen

adsorption, absorption implies the migration of hydrogen atoms into the bulk of the catalyst layer. This is in fact one of Pd's better known properties, and it is seen as one of the most promising candidates for hydrogen storage among the metals that absorbs hydrogen. It has however been shown that excessive hydrogen absorption can result in structural defects (e.g. cracks, hydrogen pockets), thus also compromising the structural integrity of the catalyst layer.

The mechanism of layer disintegration proposed above implies that all Pt_xPd_y electrocatalyst layers are susceptible to the formation of structural defects, although it does not necessarily result in layer disintegration (especially for Pt-rich compositions). In order to prevent or delay this process, the dissolution rate of Pd should be minimized or totally eliminated, if possible. To date, the effect of RTA on the stability of Pd electrodes in a H_2SO_4 electrolyte has not been studied. However, considering the significant influence of annealing on the electrochemical properties of the catalysts (evident from the different CV profiles), it is reasonable to assume that it would also have an effect on the dissolution of Pd.

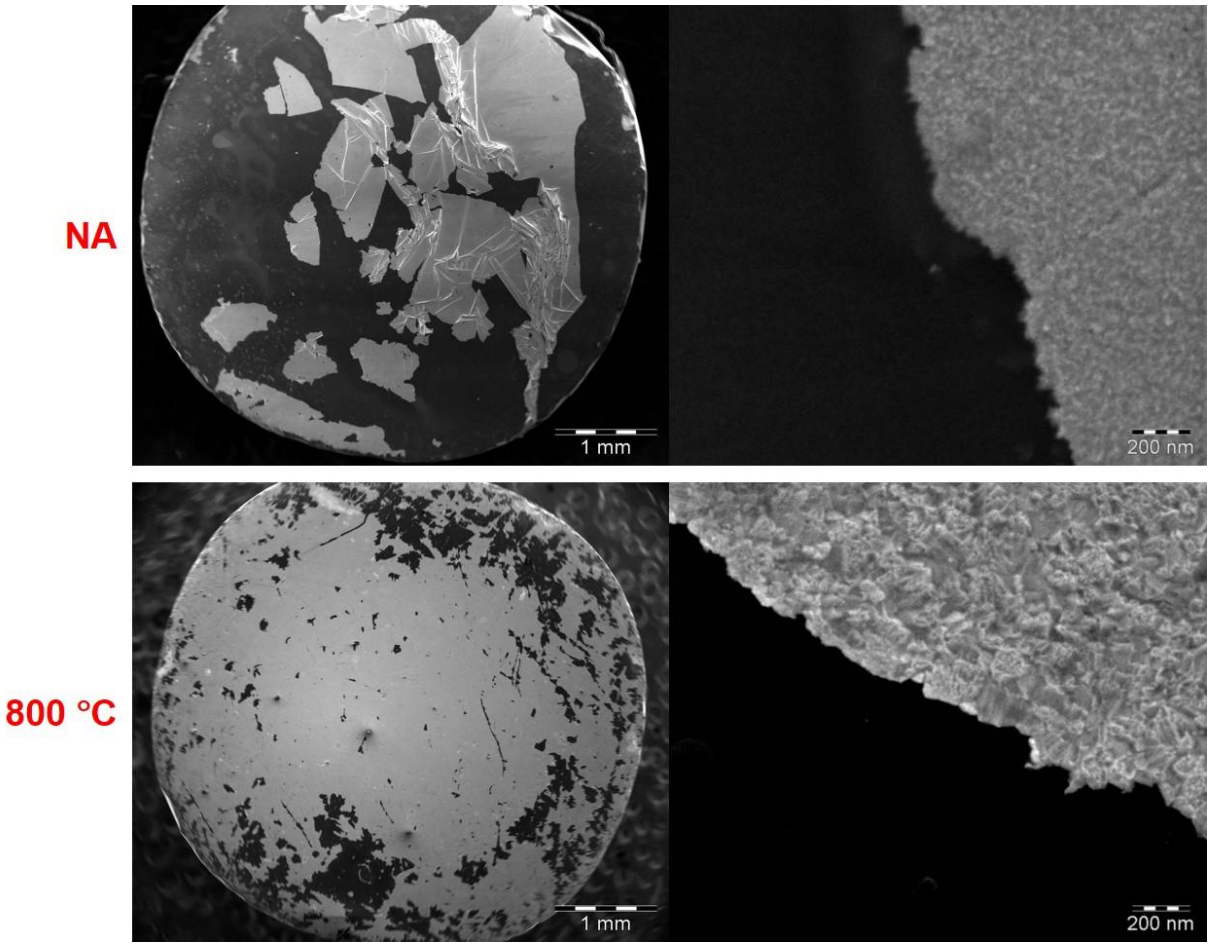

Figure 4.11: SEM micrographs of disintegrated non-annealed (NA) and annealed (800°C) Pt catalyst layers after acid stability experiments

The number of cycles obtained for the catalysts until layer disintegration was observed is shown in Table 4.8, with SEM images of the non-annealed and annealed at 800 °C Pt catalyst layers following potential cycling shown in Figure 4.11. The experiments confirmed the prediction that layer disintegration is possible for compositions containing a majority of Pt, and more importantly it also revealed that pure Pt layers ultimately disintegrate in the same fashion as the Pt_xPd_y catalyst layers. The results in Table 4.8 show that annealing generally results in increased layer stability, although both compositions exhibit a single T_{High} point where annealing did not cause a significant increase in stability (800 °C for Pt_3Pd_2), and even resulted in a slight decrease (700 °C for Pt). The majority of catalyst layers disintegrated upon rotation of the electrode (every 200 cycles), while layer disintegration of the other catalysts was observed during periodic inspections while the CV technique ran. Due to the reflectivity and smoothness of the electrode surfaces, any signs of layer disintegration (e.g. cracks, metal flakes hanging from the surface, exposed GC surface) could easily be observed by looking up at the electrode surface through the transparent glass cell. No trends in the pattern or extent of layer disintegration could be observed for either annealing temperature or composition. Layers that disintegrated upon rotation displayed a greater extent of total layer separation from the GC support (to be expected), while the other catalyst layers displayed small cracks and/or multiple points with minor total layer separation. An example of both cases is shown in Figure 4.11, with the difference clearly visible. Although the non-annealed Pt catalyst layer lasted significantly longer than the Pt_3Pd_2 counterpart, annealing increased the stability of the Pt_3Pd_2 layers to a greater extent when compared to Pt. The annealing temperature that resulted in the most stable Pt_3Pd_2 catalyst layer (800 °C) represents a three-fold increase in the number of cycles, while the most stable Pt catalyst layer (700 °C) exhibited less than a two-fold increase over the non-annealed layer. It is interesting to note that while annealing at 700 °C caused the largest increase in layer stability for Pt, it is the only annealing temperature that did not result in a significant improvement of the stability of the Pt_3Pd_2 catalyst layer. Conversely, annealing at 600 °C resulted in the second highest stability for the Pt_3Pd_2 layers while actually causing a slight decrease in the stability of the Pt catalyst layer.

Table 4.8: Cycles completed on non-annealed (NA) and annealed Pt and Pt_3Pd_2 catalysts until layer disintegration

Pt	Temperature	Pt_3Pd_2
Cycle no.		**Cycle no.**
1000	**NA**	600
900	**600 °C**	1600
1800	**700 °C**	650
1450	**800 °C**	1850
1400	**900 °C**	1400

While these results conclusively show that annealing (at the majority of T_{High} points studied) does indeed improve the stability of the Pt and Pt_3Pd_2 catalyst layers in a 1 M H_2SO_4 solution, the mechanism underlying this increase in stability remains unknown. Considering the fact that the extent of layer disintegration did not change with annealing temperature, it is very likely that annealing improves the chemical stability of Pd rather than its physical stability. Without information regarding the forces that hold the catalyst layers on to the GC support and additional analytical techniques, a definite conclusion is however impossible. Furthermore, these results show that as with activity, there is no clear correlation between the surface roughness parameters, degree of crystallinity, and crystallite size of the catalyst layers and their stability in an acidic electrolyte. Interestingly enough, a degree of correlation does exist between the catalytic activity and stability of the non-annealed and annealed Pt and Pt_3Pd_2 catalyst layers. Annealing at 700 °C resulted in the most active and stable annealed Pt catalyst layer, while annealing at 600 °C resulted in the lowest activity and stability. The same can be said of the Pt_3Pd_2 catalyst layers, where annealing at 800 °C and 700 °C, respectively resulted in the highest and lowest activity/stability of the annealed Pt_3Pd_2 catalysts. The stability experiments also indicated 800 °C as the best common annealing temperature; thus this T_{High} point was chosen to be employed in further experiments.

4.2 Rotating disc electrode experiments

4.2.1 SO_2 oxidation activity

The LP curves at five rotation rates (200, 400, 800, 1500, and 2500 rpm) of the annealed Pt and Pt_3Pd_2 catalysts are shown in Figure 4.12, with the corresponding non-annealed LP curves shown in 4.13. The curves each represents a single set of data points for the various catalysts, and at least three sets are employed in the analysis of the raw data.

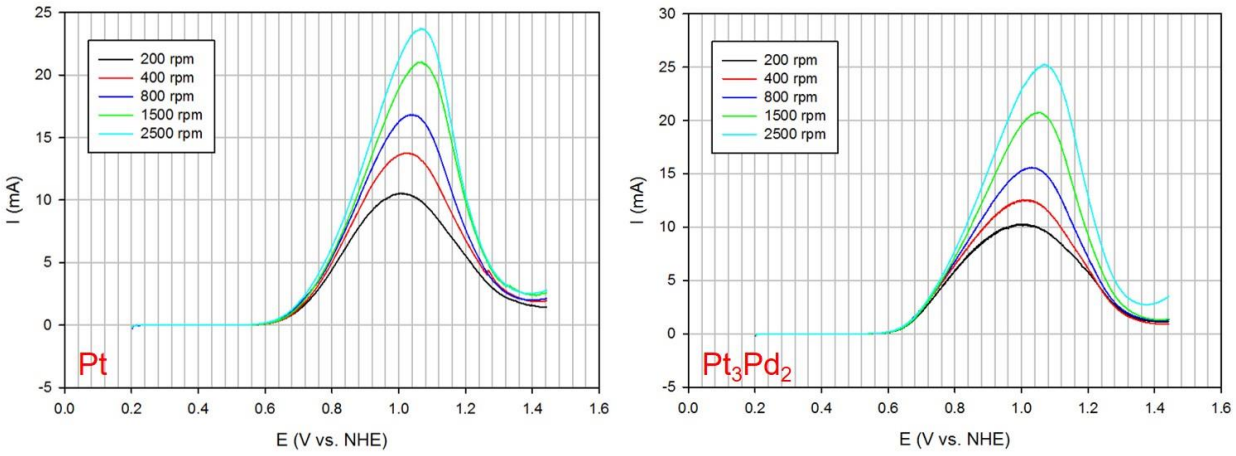

Figure 4.12: SO_2 oxidation LP curves of annealed Pt and Pt_3Pd_2 catalysts in 1 M H_2SO_4 + 100 mM SO_2 (rotating electrode, scan rate = 10 $mV.s^{-1}$)

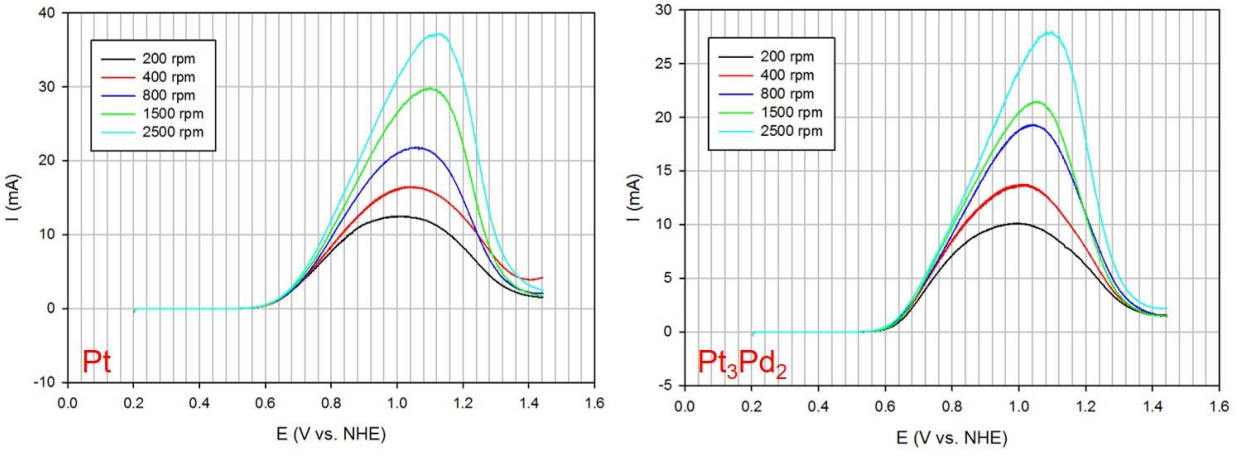

Figure 4.13: SO_2 oxidation LP curves of non-annealed Pt and Pt_3Pd_2 catalysts in 1 M H_2SO_4 + 100 mM SO_2 (rotating electrode, scan rate = 10 $mV.s^{-1}$)

What is immediately apparent from the above LP curves is that they do not follow the expected trend which is usually observed in RDE experiments in the sense that no plateau region can be observed. The decrease in current at ~1.100 V is indicative of the inhibition of the SO_2 oxidation reaction, and can be ascribed to the formation of various surface oxide species of both Pt and Pd. Although the reaction takes place in a solution with a negligible amount of dissolved oxygen (due to purging with N_2), oxygen is still present in the form of H_2O. Appleby and Pinchon (1979), as well as Lu and Ammon (1982), proposed a possible reaction pathway which involved the formation of MO_{ads} active sites (Equations 14 – 16) [10, 40]. At voltages above ~1.000 V the metals are oxidised to their corresponding metal oxides (which can be seen in Fig 4.9), which in turn inhibit the oxidation of SO_2 to H_2SO_4 [3] and result in the Bell-shaped curves seen in Fig 4.12 and Fig 4.13.

$$M + H_2O \rightarrow MOH + H^+ + e^- \quad (14)$$

$$MOH \rightarrow MO_{ads} + H^+ + e^- \quad (15)$$

$$SO_2 + H_2O + MO_{ads} \rightarrow H_2SO_4 + M \quad (16)$$

Except for the above, the curves do follow the expected trend that higher rotation rates result in steeper slopes and higher peak currents. Interestingly enough, it also appears that the peak currents seem to shift to higher potentials with increasing rotation rates. It should be noted that it proved to be difficult to acquire a valid set of data (according to the above trends), with the lower rotation rates (200 & 400 rpm) producing the most outliers (in the shape of more rounded curves with less prominent peaks). In general it was also observed that the angle of the glassy carbon electrode surface had a large effect on the results, and in order to obtain the expected trend in each series the electrode surface had to be perfectly perpendicular to the axis of rotation. Any slight deviation from this angle (due to either a bent rotation shaft, or an uneven Teflon GC electrode holder/GC catalyst surface, which can be caused by torn/damaged O-rings in the electrode holder or uneven polishing of the GC electrodes) resulted in rounder LP curves with less defined peaks and more background oscillations.

Figure 4.14 shows the different regions in a RDE voltammogram and the corresponding Tafel plot (a plot of log |I| vs. overpotential) for Set 1 of the non-annealed Pt catalyst. Each region is described by a different equation, corresponding to the varying contributions of electron transfer and mass transport to the overall reaction rate. At the equilibrium potential (described by the Nernst equation), where the net current is zero, the surface concentration of the reactant species is equal to the bulk concentration. As the voltage is increased and the rate of the reaction increases, a concentration gradient is produced due to a difference between the surface and bulk concentrations of the reactant species. The higher the voltage, the greater the concentration gradient will be.

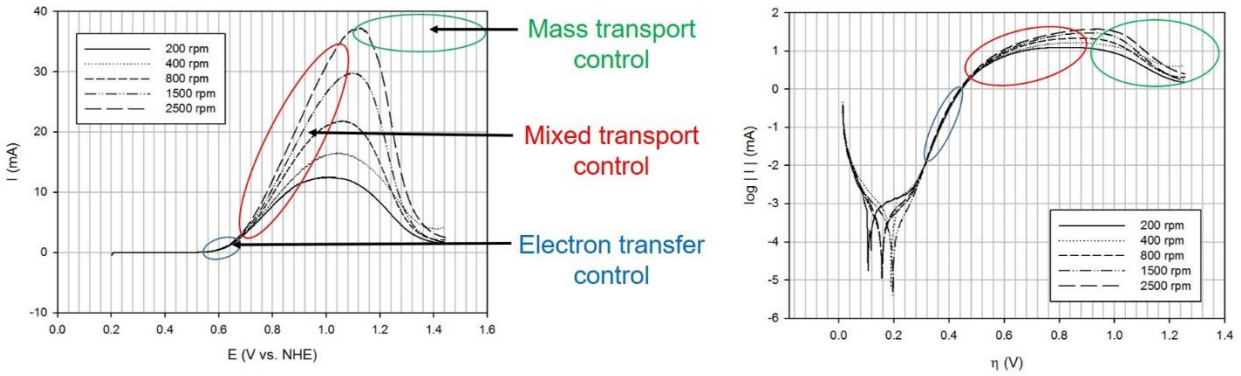

Figure 4.14: Regions of electron transfer and mass transport control shown on a LP curve and Tafel plot of SO_2 oxidation on a non-annealed Pt catalyst at different rotation rates

Close to the equilibrium potential (E_e), where the net current is small and the rate of the reaction is slow (thus also the rate of electron transfer), the current varies with potential and is not dependent on the rotation rate of the electrode. Thus, the rate of electron transfer is the rate-determining step, which is called kinetic control. In this low overpotential region, the system is under pure electron transfer control (which implies surface and bulk concentrations of species are identical), and the relationship between the current and potential is described by the Butler-Volmer and Tafel equations (Equation 9 and Equation 17, respectively). The Tafel equation features two constants: a (Equation 18) and b (Equation 19). In a Tafel plot the slope of the line is known as the Tafel slope, and in the case of an anodic reaction is described by Equation 20. From the intercept of this plot it is also possible to calculate the exchange current density (i_0). The Tafel equation is only valid if no mass transport effects are present and if the back reaction is less than 1% of total current ($|\eta| > 0.118$ V at 25 °C/323.15 K) [24].

$$\eta = a + b \log |i| \tag{17}$$

$$a = \frac{2.3RT}{(1-\alpha)F} \log i_0 \tag{18}$$

$$b = \frac{2.3RT}{(1-\alpha)F} \tag{19}$$

$$Slope = \frac{(1-\propto)F}{2.3RT} \tag{20}$$

At intermediate overpotentials, mass transport of the reactant species begins to play a role, and the contributions of the rates of electron transfer and mass transport to the total reaction rate are similar (mixed transport control). In this region, the current is dependent upon both the potential and electrode rotation rate, and in this situation the current-potential relationship is described by the Koutecky-Levich equation (Equation 21). This equation introduces three new parameters, with D_R the diffusion coefficient of species R, v_R the kinematic viscosity of species R, and ω the

rotation rate of the electrode in radians.s^{-1} (Equation 22). The bottom coefficient in the first term of the Koutecky-Levich equation is also known as the kinetic current (I_k), with the relation shown in Equation 23. This equation is only valid for a slow electron transfer process, where the surface concentration is equal to the bulk concentration of species R (thus the kinetic control region).

$$\frac{1}{I} = \frac{1}{nF\pi r^2 k^0 C_R} + \frac{1}{0.62nF\pi r^2 D_R^{2/3} v_R^{-1/6} C_R} \frac{1}{\sqrt{\omega}} \quad (21)$$

$$\omega = 2\pi\left(\frac{rpm}{60}\right) \quad (22)$$

$$I_k = nF\pi r^2 k^0 (C_R)_{x=0} \quad (23)$$

At higher potentials (high overpotentials), where the reaction/electron transfer rate is very high, mass transport plays a significant effect and becomes the limiting step (mass transport control). The current is only dependent on the rotation rate (independent on potential), and the current-potential relationship in this region is described by the Levich equation (Equation 24), where I_L is known as the limiting current.

$$I_L = 0.62nF\pi r^2 D_R^{2/3} v_R^{-1/6} C_R \sqrt{\omega} \quad (24)$$

Substitution of Equation 23 (Levich equation) and Equation 22 into Equation 20 (Koutecky-Levich equation) yields another form of the Koutecky-Levich equation (Equation 25).

$$\frac{1}{I} = \frac{1}{I_k} + \frac{1}{I_L} \quad (25)$$

Theoretically, the exchange current can also be determined if the value of I_k is determined at different potentials with a graph of log I_k vs. η (Equation 26) [41].

$$\log I_k = \log I_0 + \frac{\alpha nF}{2.3RT}\eta \quad (26)$$

Levich and Koutecky-Levich analysis

In order to perform the Koutecky-Levich analysis the limiting current should first be obtained, and the Levich analysis should be done to confirm that the system is indeed under mass transport control. If the system is under complete mass transport control, a plot of I_L vs. $\omega^{1/2}$ will yield a straight line that passes through the origin. Immediately, the data from all the electrocatalyst thin films (both annealed and non-annealed) presents a problem: The region where current is only dependent on rotation rate (mass transport control) is not observed in any of the data sets. This is due to the inhibition of the SO_2 electro-oxidation reaction mentioned above. Usually, the limiting current for the various rotation rates would be obtained from a single potential point (fixed). In this case, the 'limiting current' was defined as the maximum current value obtained from the LP curves. Since there is a peak shift, the 'limiting current' for each rotation rate would be read from

different potential points. The data from the Pt and Pt_3Pd_2 catalysts are shown in Table 4.9 and Table 4.10, respectively, while the corresponding plots of I_L vs. $\omega^{1/2}$ can be seen in Figure 4.15.

Table 4.9: 'Limiting current' and potential of non-annealed and annealed Pt catalysts at 5 rotation rates

Parameter	**Non-Annealed**		**Rotation rate (rpm)**	**Annealed**	
	Value	Std.Dev.		Value	Std.Dev.
I_L (mA)	12.220	0.260	**200**	10.390	0.660
	15.886	0.729	**400**	14.108	0.651
	20.617	1.209	**800**	17.157	1.216
	26.652	2.761	**1500**	20.682	1.702
	33.308	3.611	**2500**	22.719	1.718
E_p (V)	1.009	0.006	**200**	1.008	0.002
	1.036	0.005	**400**	1.023	0.003
	1.056	0.010	**800**	1.040	0.004
	1.087	0.016	**1500**	1.062	0.006
	1.108	0.017	**2500**	1.060	0.007

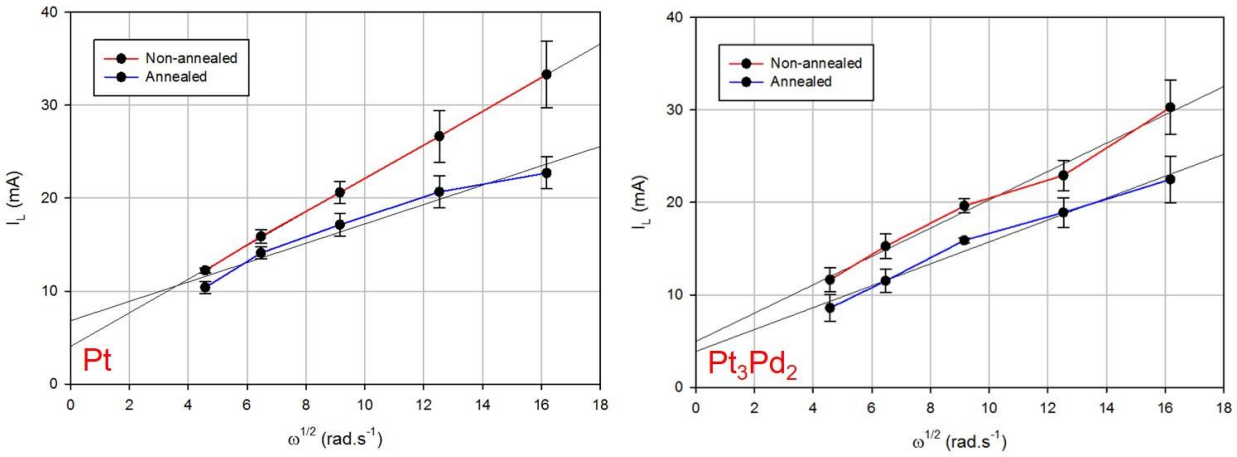

Figure 4.15: **I_L vs. $\omega^{1/2}$ plots of non-annealed and annealed Pt and Pt_3Pd_2 catalysts for Levich analysis (different potentials, shown with 95% confidence regression line)**

Table 4.10: **'Limiting current' and potential of non-annealed and annealed Pt_3Pd_2 catalysts at 5 rotation rates**

Parameter	Non-Annealed		Rotation rate (rpm)	Annealed	
	Value	Std.Dev.		Value	Std.Dev.
I_L (mA)	11.646	1.327	**200**	8.591	1.478
	15.263	1.302	**400**	11.514	1.255
	19.633	0.772	**800**	15.892	0.287
	22.931	1.647	**1500**	18.917	1.601
	30.275	2.927	**2500**	22.492	2.509
E_p (V)	1.008	0.021	**200**	1.003	0.005
	1.019	0.010	**400**	1.018	0.011
	1.037	0.008	**800**	1.036	0.011
	1.066	0.010	**1500**	1.050	0.007
	1.095	0.004	**2500**	1.068	0.003

The data in Tables 4.9 and 4.10 clearly show that the 'limiting current'/peak current shifts towards higher voltages as the rotation rate is increased. This trend is observed for all electrocatalyst thin films through all rotation rates, with the only exception being the annealed Pt catalyst at 2500 rpm, which is slightly lower than the potential at 1500 rpm. The increase in 'limiting current' with increasing rotation rate is also observed for all catalysts at all the rotation rates. The graphs in Figure 4.15 however indicate that none of the catalysts are under complete mass transport control. The plots are all curved (with the exception of non-annealed Pt), with both non-annealed and annealed Pt_3Pd_2 catalysts also displaying one inflection point each. Although non-annealed Pt displays a straight line, its regression line does not intersect with the origin, which also holds true for the other catalysts. The regression lines were added to the plots in SigmaPlot 12 using a 95% confidence interval. This proves that none of the catalysts systems are under mass transport control, which indicates that some part of the current can still be attributed to electron transfer/kinetic control. It follows logically that the true limiting currents in the various catalyst systems would lie at voltages higher than the maximum peak potentials observed for each of the catalysts. However, due to the inhibition of SO_2 oxidation by the formation of surface oxides, the limiting currents are impossible to determine. To ensure the validity of this conclusion, a second Levich analysis was performed using current values obtained from a fixed potential point (which is how the analysis is usually done). This potential point was chosen as the average potential of the peak potentials at the different rotation rates (Tables 4.9 and 4.10) for each of the catalysts. The data can be found in Table 4.11 with a visual representation shown in Figure 4.16. The second analysis confirmed the conclusion obtained from the first analysis, and it can be stated with certainty that none of the catalyst systems are under total mass transport control. It follows logically that the 'limiting currents' (I_L) given in Tables 4.9 to 4.11 are invalid, as they are not accurate representations of the true limiting currents.

Due to the fact that the true limiting current at any of the rotation rates cannot be obtained for any of the thin film electrocatalysts, Koutecky-Levich analysis of the data would be meaningless. Usually, a plot of 1/I vs. the inverse of $\omega^{1/2}$ will produce a straight line, which enables the determination of the diffusion constant or number of electrons exchanged from the slope, as well as calculation of the kinetic current from the intercept. Since the true values of I_L are not known for any catalyst in this case, the results obtained from this analysis would not be valid (no matter which potentials in the mixed control region are employed in the analysis); if the contribution of the mass transport component (I_L) to the total reaction rate (I) is unknown, the value of the electron transfer component (I_k) can't be determined (see Equation 25). Thus, it is impossible to compute the true exchange currents for the oxidation of aqueous SO_2 on the various thin film electrocatalysts with this method. Levich and Koutecky-Levich analysis of SO_2 oxidation data obtained from RDE experiments would only be applicable to catalysts which do not exhibit the SO_2 oxidation inhibition behaviour seen in the catalysts employed in this study.

Table 4.11: 'Limiting current' of non-annealed and annealed Pt and Pt_3Pd_2 catalysts at 5 rotation rates (fixed potential point)

Catalyst	Non-Annealed		Rotation rate (rpm)	Annealed	
	Value	Std.Dev.		Value	Std.Dev.
Pt	11.929	0.275	**200**	10.259	0.611
	15.621	0.859	**400**	14.035	0.677
	20.532	1.217	**800**	17.110	1.197
	26.252	2.454	**1500**	20.360	1.681
	32.068	3.127	**2500**	22.288	1.506
	I_L (mA)			**I_L (mA)**	
Pt_3Pd_2	11.395	1.411	**200**	8.430	1.451
	15.036	1.479	**400**	11.405	1.200
	19.555	0.748	**800**	15.838	0.261
	22.785	1.587	**1500**	18.773	1.551
	29.301	2.981	**2500**	21.893	2.395

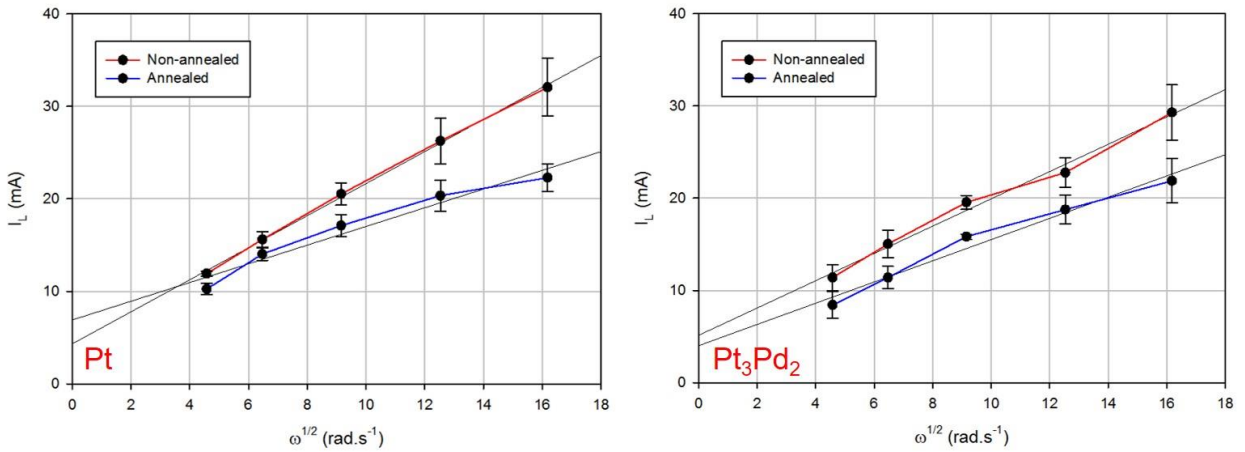

Figure 4.16: I_L vs. $\omega^{1/2}$ plots of non-annealed and annealed Pt and Pt_3Pd_2 catalysts for Levich analysis v2 (fixed potentials, shown with 95% confidence regression line)

Tafel analysis

Although the Tafel equation (Equation 17) is frequently used in various electrochemical studies, most papers do not take all the assumptions of the equation into account. As mentioned above, the equation assumes that the net current only consists of the kinetic component (i.e. electron transfer/kinetic control) and that no mass transport effects are present. Furthermore, the back reaction must account for less than 1% of the total current (I), which translates to overpotentials larger than 0.118 V at a temperature of 298.15 K (25 °C). RDE experiments are thus a requirement for the use of the Tafel equation, since it is possible to identify an overpotential region where the back reaction is as small as possible, yet no mass transport effects are present (current still independent of rotation rate). For every reaction, there exists a certain potential range where the current-potential relationship can accurately be described by the Tafel equation. In these potential ranges (which will be referred to as Tafel regions) the system will display Tafel behaviour, where the LPs at the various rotation rates will display identical currents (i.e. all lines lie on top of each other) and first order function/straight line behaviour in a plot of log |I| vs. η (Tafel plot, see Equation 17). If these regions can be identified in the various Tafel plots, the exchange current density (i_0) can be calculated from the intercept (a, as described by Equation 18), while the Tafel slope (b, as described by Equation 19) can be obtained from the slope of the straight line.

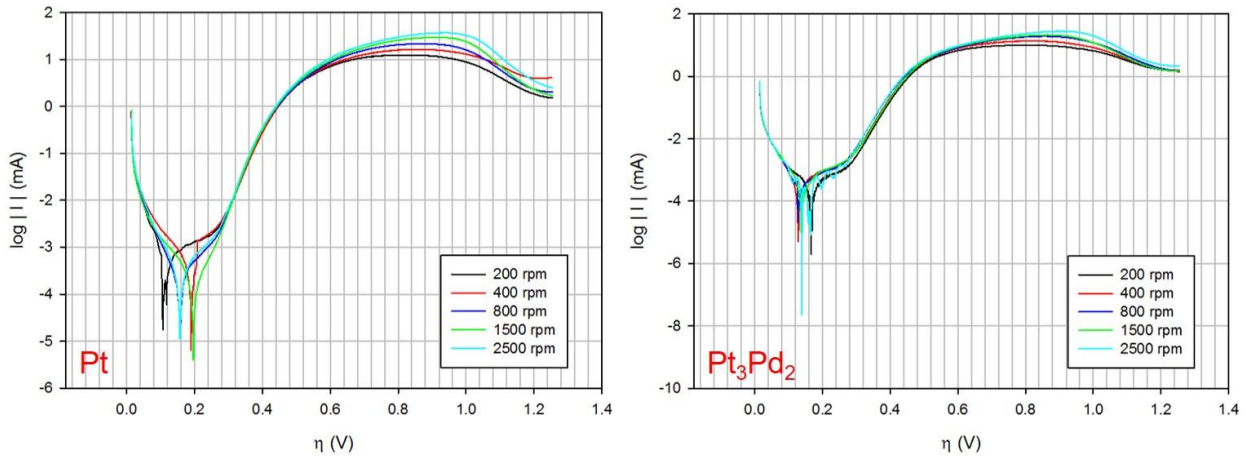

Figure 4.17: Tafel plots of non-annealed Pt and Pt_3Pd_2 catalysts in 1 M H_2SO_4 + 100 mM SO_2 (rotating electrode, scan rate = 10 mV.s^{-1}, Set 1)

An example of Tafel plots over the entire scan range for Set 1 of both Pt and Pt_3Pd_2 (non-annealed) can be seen in Figure 4.17. The graphs illustrate that although the plots of Pt and Pt_3Pd_2 differ, they follow the same form and that Tafel behaviour might be found in the overpotential range of ~0.300 – 0.600 V. The overpotential is calculated with Equation 7, and in

these experiments the equilibrium potential (Equation 8) is determined to be 0.188 V (when C_O = [1] = 1 M H_2SO_4, C_R = [0.1] = 100 mM SO_2, T = 298.15 K, and n = 2). In order to identify the Tafel region for each catalyst, Tafel plots with consecutively smaller ranges are plotted so that the plots can be studied in finer detail to enable visual determination of the potential ranges which exhibit Tafel behaviour. Figure 4.17 shows the Tafel plots of the Pt and Pt_3P_2 (both non-annealed and annealed) catalysts over the overpotential range of 0.300 - 0.800 V.

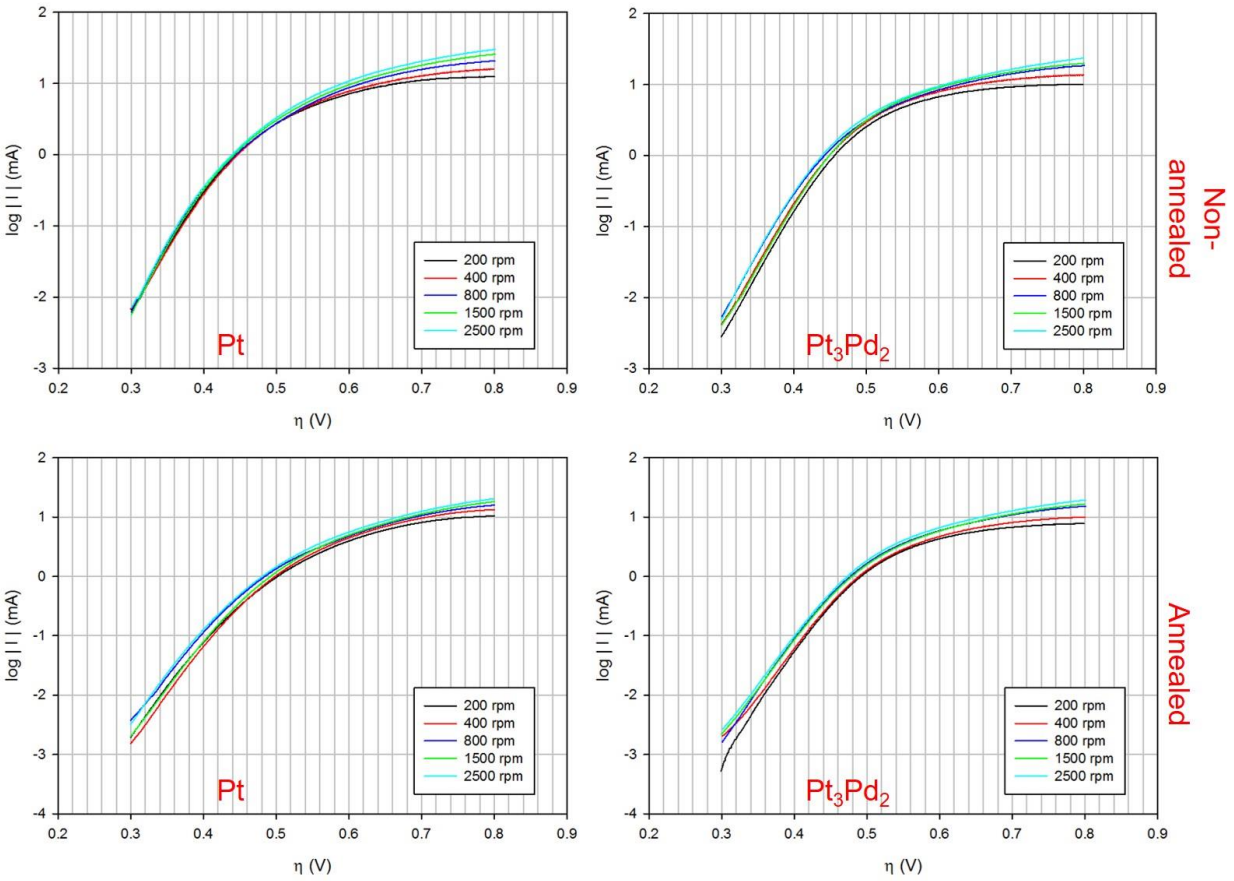

Figure 4.18: Tafel plots of Pt and Pt_3Pd_2 (non-annealed and annealed) catalysts in 1 M H_2SO_4 + 100 mM SO_2 (rotating electrode, scan rate = 10 mV.s^{-1}, Set 1)

The plots in Figure 4.18 reveal that although Tafel behaviour (straight lines) is exhibited by the catalysts in the overpotential region of approximately 0.300 - 0.440 V, there are slight variations in the current between the various rotation rates in this region. This can be attributed to the fact that the ECSAs of the electrodes of a given catalyst are not exactly identical (although the geometric area is) due to variations in the surface morphology on an atomic scale. Closer investigation over this overpotential range for all data sets of the catalysts revealed that the two Pt catalysts displayed Tafel behaviour in the overpotential range of 0.320 – 0.380 V, while this range was larger for the Pt_3Pd_2 catalysts (0.320 – 0.420 V). Due to the slight variations in current

in these overpotential regions, only three rotation rates which resulted in the most identical lines (current-overpotential behaviour) were employed in the analysis (unique to each set of the various thin film catalysts) to ensure the most accurate results. Tafel analysis of the data sets of the catalysts was thus conducted in the overpotential region of 0.330 – 0.380 V (330 – 380 mV) for the various thin film catalysts.

Multiple linear regression was done on the each set of data in order to obtain 3 straight lines for each thin film catalyst. The linear regressions were performed in SigmaPlot using the global curve fit tool, with the parameters set to 1st Order regression and shared slopes and intercepts. Only regression lines with a coefficient of determination ($R^{2(1')}$) of 0.900 or higher were accepted to be valid and useable in the analysis. With three straight lines obtained for every catalyst the exchange current densities (i_0) and Tafel slopes could be calculated for each thin film catalyst, which enables the calculation of the averages as well as their corresponding standard deviations. The coefficients of determination for each set of data for all the catalysts can be seen in Table 4.12.

Table 4.12: Coefficients of determination obtained from multiple linear regression on all data sets in SigmaPlot

	R^2 (Set 1)	**R^2 (Set 2)**	**R^2 (Set 3)**
Pt NA	0.994	0.987	0.900
Pt A	0.953	0.998	0.981
Pt_3Pd_2 NA	0.916	0.987	0.959
Pt_3Pd_2 A	0.972	0.980	0.947

The table above indicates that the data from the RDE experiments are relatively well defined by the various regression lines obtained by multiple linear regression. Although all values are equal or above the 0.900 mark, only two values reach 0.990 or above, which would be seen as ideal. The lower values are almost exclusively a product of small differences in the currents at the various rotation rates, with the vast majority of Tafel plots displaying only parallel lines and virtually no intersecting lines (differing slopes). This indicates that the various systems are under pure electron transfer/kinetic control in this overpotential region (330 – 380 mV). The reason that most of the plots display parallel lines can be attributed to the fact that the current was not normalised for the ECSA (the determination of which falls beyond the scope of this study) of the various electrodes. Differences in the observed current between the electrodes of a certain catalyst are thus to be expected. This is illustrated in Figure 4.19, which shows the three rotation rates

employed in the Tafel analysis of the first set of both Pt and Pt_3Pd_2 (non-annealed) and the two corresponding regression lines.

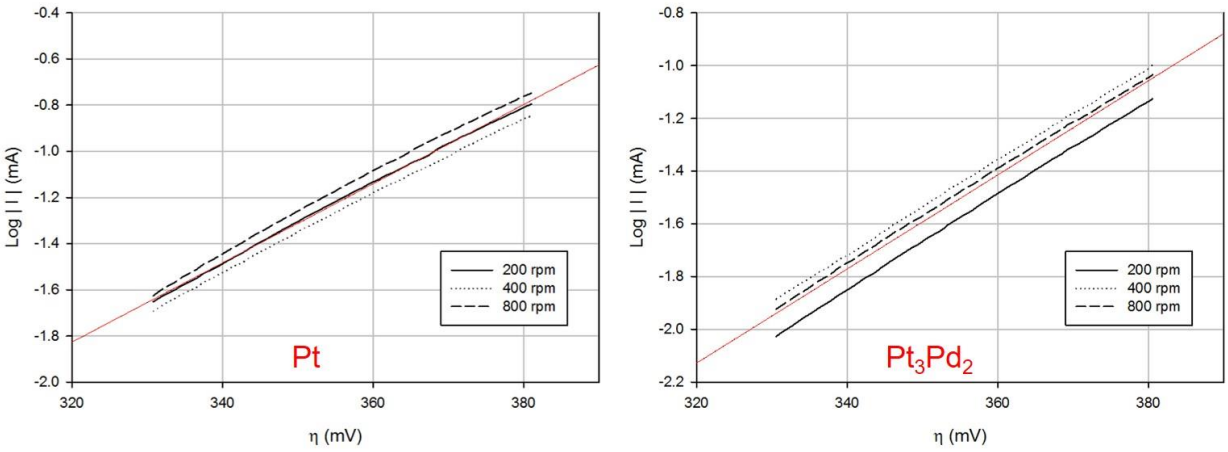

Figure 4.19: Tafel plots with regression lines of non-annealed Pt and Pt_3Pd_2 catalysts in 1 M H_2SO_4 + 100 mM SO_2 showing the parallel and straight line behaviour at the rotation rates employed in the analysis (rotating electrode, scan rate = 10 mV.s^{-1}, Set 1)

The parameters of the regression lines are stored in a report file, which SigmaPlot generates upon completion of every multiple linear regression task. From this file the important parameters (coefficient of determination, intercept, and slope) can be copied into Windows Excel to enable the calculation of the exchange current densities and Tafel slopes (see Appendix). The averages and standard deviations of these values are determined at the end of the calculation process. To calculate the exchange current density for a set, the intercept value is raised to the power of ten ($10^{\text{intercept value}}$), after which this value is normalised with geometric area (A = 0.196 cm^2 for a GC electrode with a 5mm diameter) and converted to a manageable quantity (pA in this case). The Tafel slope can easily be obtained by taking the reciprocal of the slope value of the regression line (1/slope value). The peak current density, peak potential, onset potential (activity parameters determined in Section 4.1.2), together with the exchange current density and Tafel slope (kinetic parameters) of the four thin film catalysts are given in Table 4.13.

Table 4.13: Activity and kinetic parameters for non-annealed and annealed Pt and Pt_3Pd_2 catalysts

Catalyst	Non-Annealed		Parameter	Annealed	
	Value	Std.Dev.		Value	Std.Dev.
Pt	17.471	1.325	**i_P (mA.cm^{-2})**	11.090	3.212
	0.762	0.011	**E_P (V)**	0.829	0.009
	0.601	0.002	**E_i (V)**	0.651	0.010
	196.130	34.044	**i_0 (pA.cm^{-2})**	121.848	23.845
	58.714	0.721	**Tafel slope (mV.dec^{-1})**	61.351	0.376
Pt_3Pd_2	19.327	0.954	**i_P (mA.cm^{-2})**	14.179	0.518
	0.735	0.009	**E_P (V)**	0.786	0.008
	0.601	0.004	**E_i (V)**	0.637	0.004
	99.528	12.358	**i_0 (pA.cm^{-2})**	82.410	6.197
	55.664	0.642	**Tafel slope (mV.dec^{-1})**	59.289	0.203

As mentioned in Section 2.3 the exchange current density is directly related to the standard rate constant, thus higher values of i_0 imply faster kinetics. However, this is not the only useful kinetic parameter that can be obtained from a Tafel analysis. The Tafel slope is also a good indicator of the reaction kinetics for a specific system, with lower values indicating more favourable reaction kinetics and vice versa [3]. As can be seen from Table 4.13 the two Pt thin films have the highest exchange current density, with the non-annealed catalyst displaying a higher value than its annealed counterpart. This trend also holds true for the Pt_3Pd_2 thin film catalysts, although the relative difference is much smaller when compared to Pt (~20% decrease for Pt_3Pd_2 vs. a ~60% decrease for Pt). Accurate comparison of the exchange current density values is however difficult due to the large standard deviations associated with the various values. This problem can be resolved if the ECSA of all the electrodes used in the RDE experiments can be determined accurately. Nevertheless, the exchange current densities do still reveal an important fact. Their low values (all in the pA.cm^{-2} range, thus mA.cm^{-2} x 10^{-9}) indicate that the SO_2 electro-oxidation reaction is indeed very sluggish, which is why such large overpotentials are required to drive the

reaction at an acceptable rate. The exchange current densities calculated with the Tafel analysis are also in the same range as those that can be found in literature (only papers in which the analysis was conducted correctly and the assumptions of the Tafel equation was observed). Appleby & Pinchon (1979) reported an exchange current of 10 $pA.cm^{-2}$ with a Tafel slope of 28 $mV.dec^{-1}$ for a Pt catalyst in 44% H_2SO_4, 0.42 M SO_2 and 50 °C (348.15 K) [40]. With such extremely low values, a two-fold increase in this range will not have a significant effect on the overpotential required to drive the reaction at a certain rate. Definite improvements in activity will only be observed when the exchange current density is several orders of magnitude larger than $pA.cm^{-2}$.

Apart from the exchange current densities, Table 4.13 also reveals an interesting trend that provides a link between the kinetic and activity parameters of the thin film catalysts. While exchange current does not seem to directly dictate the electrolytic activity displayed by the various catalysts in the stationary electrode experiments (e.g. although non-annealed Pt has a much higher i_0 value than Pt_3Pd_2, Pt_3Pd_2 displays similar or better activity parameters when compared to Pt), the data suggests that a link between the Tafel slope and the activity of the thin film catalysts does exist. Non-annealed Pt_3Pd_2 has the lowest Tafel slope (55.664 $mV.dec^{-1}$) of all the catalysts that were tested, and as can be seen in Table 4.13 it exhibits a higher peak current density than Pt, with an identical onset potential and lower peak potential. Conversely, the catalyst with the highest Tafel slope value (annealed Pt, 61.351 $mV.dec^{-1}$) displays the poorest activity parameters, even though it has a higher exchange current density than both Pt_3Pd_2 catalysts. In the case of SO_2 electro-oxidation systems, which have extremely low exchange current density values, the Tafel slope appears to be the more applicable kinetic parameter when predicting the actual electrolytic activity that will be observed at the higher applied potentials employed in electrolysis cells. In systems such as these, where very large overpotentials are required to bring about any meaningful flow of net current (due to the extremely low i_0 values), the Tafel slopes can be used to determine the optimal operating conditions and catalysts for the system in question. The Tafel slope can thus be seen as a kinetic parameter that predicts the activity of a reaction system at high overpotentials. The applicability and usefulness of Tafel slopes with systems that have high exchange current densities (thus requiring a small overpotential) remain to be seen.

In the case of electrocatalyst development for SO_2 electro-oxidation the Tafel slopes are however very useful in determining the suitability of a given catalyst and predicting its electrolytic activity. The Tafel slopes obtained in this study clearly show that the non-annealed Pt_3Pd_2 catalyst is superior to the Pt catalyst in terms of activity, and that the process of annealing these thin film catalysts at 800 °C negatively affects both the reaction kinetics and activity parameters (confirmed by the activity values determined earlier in the study). Furthermore, if the Tafel slope of Pt (58.714 $mV.dec^{-1}$) is compared to the Tafel slope reported by O'Brien *et al.* (2010) it is possible to infer

that under identical operating conditions (74 mV.dec^{-1}; Pt electrode in 1 M H_2SO_4 + 0.1 M SO_2 at 25 °C) [42], a sputtered thin film on a GC electrode is superior to the corresponding bulk electrode catalyst. In conclusion, while catalysts with higher exchange current densities (and thus higher standard rate constants) are favourable, for a process such as SO_2 electro-oxidation the development of catalysts with lower Tafel slopes are more important since the exchange currents are so low (unless catalysts can be developed that increase this value by several orders of magnitude).

4.2.2 SO_2 oxidation stability

Originally, the SO_2 oxidation stability experiments were designed to be quantitative in nature; however, due to health/medical reasons only a few preliminary runs were completed. Unfortunately, not enough data was generated to produce accurate and repeatable quantitative results; thus these experiments will only be presented in a qualitative manner. The experiments that were successfully completed did however still employ the setup and settings that were discussed in Sections 3.4.2 and 3.5.4, respectively. The goal of these experiments was to determine the stability/durability of the Pt and Pt_3Pd_2 thin film catalysts under 'real world' working conditions (i.e. actively oxidising SO_2 while a constant potential is applied). Unlike the acid stability experiments, these experiments monitored current, which is directly proportional to the reaction rate and thus also the amount of product being formed. By monitoring the current over time in an 'emulated' electrolyser the performance of the various catalysts can be monitored and conclusions can be drawn about how the stability of the two catalysts compositions, as well as the effect of annealing, compare to each other.

All CAs displayed similar trends, with the current at its highest at the start of the experiment, after which the current immediately fell exponentially to approximately half its peak value within 10 - 20 minutes, followed by a more stable phase that lasted for the rest of the experiment (displayed in Fig 4.20). The reason for this sudden drop in current is unclear; however, it can most likely be attributed to the fact that the setup had to be continually adjusted upon initiating the CA, with both the water and gas flow (thus also pressure) requiring fine tuning for approximately 30 minutes until the closed system reached equilibrium (constant water level in the cell). Another possibility is that the catalyst layers were poisoned with adsorbed sulphur species, thus blocking some of the active sites. While all the catalyst samples that were tested exhibited this trend, the rate at which the current fell in the 'stable' phase did differ between the various catalysts. Due to the abovementioned phenomenon the initial current was taken as the current value at t = 2 000 s (33.33 minutes), thus enabling a more meaningful comparison between the catalysts.

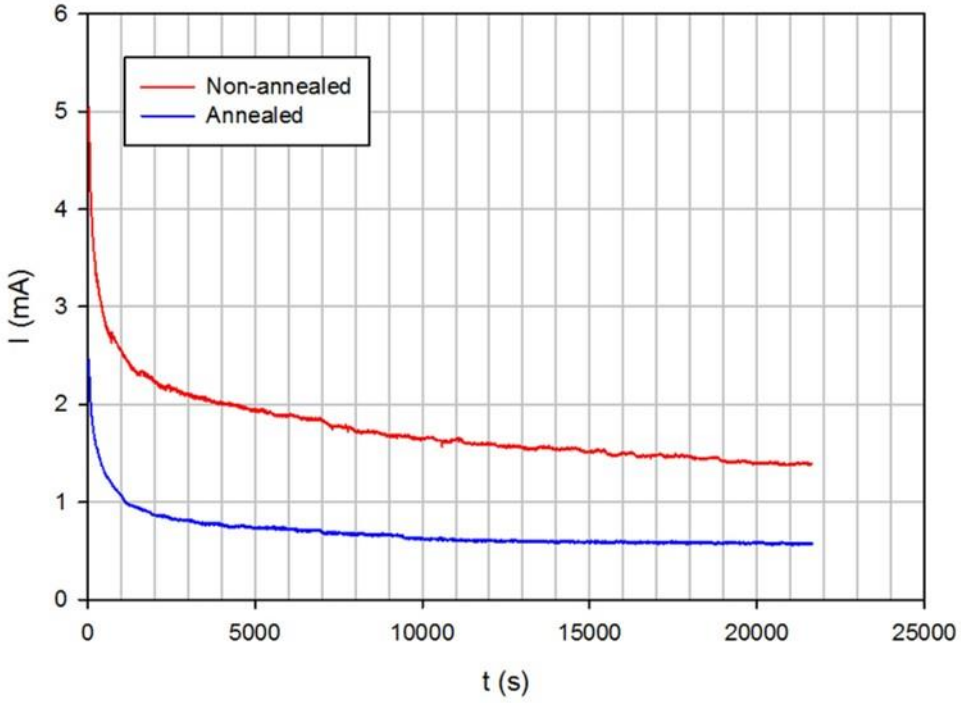

Figure 4.20: Current vs. time plot of Pt_3Pd_2 catalysts obtained with the SO_2 oxidation stability experiments

The non-annealed Pt catalysts displayed superior stability when compared to their Pt_3Pd_2 counterparts, with the Pt electrodes maintaining their current more efficiently than the Pt_3Pd_2 electrodes. Although the current did continue to drop throughout the experiment, the rate at which the current decreased was much lower for Pt when compared to Pt_3Pd_2. Over the course of approximately 5.5 hours (19 600 s) the Pt_3Pd_2 catalysts maintained between 43% and 62% of their initial currents, while the Pt catalysts maintained between 63% and 71% of their initial currents over the same time period. Furthermore, two of the Pt catalysts were subjected to longer periods in order to determine if the catalyst layers would begin to disintegrate (as was the case with the acid stability experiments). The first was subjected to an extra 18 000 s directly after the first CA experiment ended, while 36 000 s was added to the run time of the second electrode (for a total of 57 600 s = 16 hours). No signs of layer disintegration could be observed for either of these electrodes, and the second electrode managed to maintain 56% of its initial current after a run time of 15.5 hours.

Although the effect of annealing on the SO_2 oxidation stability of the thin film catalysts was the primary focus of these experiments, the process could unfortunately only be performed on 2 annealed Pt_3Pd_2 catalysts and one Pt catalyst. The two annealed Pt_3Pd_2 electrodes maintained 58% and 63% of their initial currents during the course of the experiment, while the annealed Pt electrode only maintained 44% of its initial current. In comparison to their non-annealed

counterparts, the Pt_3Pd_2 catalysts displayed enhanced stability while the stability of the Pt catalyst decreased. It should be noted that because there is not a high enough degree of repeatability for the annealed catalysts this data should be considered in a qualitative manner. However, even with the limited data it can be stated that annealing at 800 °C most likely negatively effects the SO_2 oxidation stability of Pt thin film catalysts, and it has no effect (or possibly even a positive effect) on Pt_3Pd_2 thin film catalysts. In order to draw definite conclusions more data sets are required as well as longer experimental times (at least 24 hours). The results obtained from the SO_2 oxidation stability experiments are given in Table 4.14.

Table 4.14: Percentage of initial current (current at t = 2 000 s) maintained after 6 hours by the Pt and Pt_3Pd_2 catalysts in SO_2 oxidation stability experiments

Catalyst	**Non-annealed**		**Annealed**
	Current retention (%)		Current retention (%)
Pt	65.534	1	43.968
	63.240	2	-
	71.117	3	-
	66.630	**Average**	43.968
	4.051	**Std.Dev**	-
Pt_3Pd_2	62.169	1	58.333
	43.009	2	66.303
	53.323	3	-
	52.834	**Average**	62.318
	9.590	**Std.Dev**	5.636

5 CONCLUSION

5.1 Concluding remarks

The focus of this study was to determine the electrocatalytic activity of sputtered Pt and various Pt_xPd_y thin film catalysts towards the electro-oxidation of aqueous SO_2 in a H_2SO_4 solution (also known as the SO_2-depolarised electrolysis/SDE reaction), as well as the effect of rapid thermal annealing (RTA) on the activity and stability of these catalysts. Although various aspects of the SDE reaction has been studied for decades, relatively little research has been done on electrocatalyst development. The SDE reaction forms part of the hybrid sulphur (HyS) cycle, a two-step thermoelectric cycle that is seen as one of the most promising processes for large-scale hydrogen production. While the HyS cycle appears very promising in theory, industrial application of this process is hampered by the inefficiency of the SDE electrolyser, which is largely due to the high overpotential required to drive the SDE reaction at acceptable rates. Development of electrocatalysts with improved kinetic and activity properties is crucial for the eventual industrial application of the SDE electrolyser and the HyS process. Besides the use of stationary electrode experiments, which are usually employed to determine the electrocatalytic activities of the various sputtered thin film catalysts, rotating disc electrode (RDE) experiments were also conducted to investigate the stability and kinetic properties of the most promising catalysts.

Initial experiments on a range of binary Pt_xPd_y (as well as pure Pt and Pd) thin film catalysts revealed that Pd and Pd-rich binary catalysts are not suitable for the electro-oxidation of SO_2 due to the poor stability/durability exhibited by these catalyst layers. While their performance were approximately identical to Pt (or in some cases better), the instability of these catalysts (manifested as disintegration of the sputtered thin film catalyst layers) excluded them from further experiments. The stability problems experienced with these catalysts was determined to be a result of the electrodissolution of Pd in the acidic solutions. These initial experiments did however reveal that Pd and Pt_xPd_y catalysts have electrocatalytic properties comparable to pure Pt, with activity parameters approximately equal to those displayed by Pt. While Pt (and Pt_3Pd_2) exhibited the lowest onset potentials (E_i = 0.601 V), Pt_3Pd_2, Pt_2Pd_3 and Pt_1Pd_4 displayed lower peak potentials (E_P = 0.762 V for Pt) as well as higher peak current densities (i_P = 17.471 $mA.cm^{-2}$) when compared to Pt. The onset potentials of these binary catalysts were however found to be only slightly higher than that of Pt, the highest being only 15 mV above that of Pt (Pt_1Pd_4, E_i = 0.616 V). Pd and Pt_1Pd_9 meanwhile displayed relatively higher onset potentials when compared to the above mentioned catalysts, with their peak potentials also higher than Pt, as well as lower

peak current densities. Based on the results of these experiments it was concluded that Pt_3Pd_2 was the best catalyst to be employed in further experiments (alongside Pt).

Following the development of stable temperature programs, rapid thermal annealing was employed to determine the best annealing temperature to be used in the RDE experiments, as well as the effect of annealing at the different temperatures on the surface properties, activity and stability of the Pt and Pt_3Pd_2 catalyst layers. Scanning electron microscopy/Energy-dispersive X-ray spectroscopy (SEM/EDX) analysis revealed that annealing did not alter the atomic composition of the catalyst layers, but it did however have a profound effect on the surface morphology of both Pt and Pt_3Pd_2 thin film catalysts. SEM micrographs showed significant changes in the grain sizes and grain boundaries, with higher annealing temperatures resulting in larger grain sizes and better defined grain boundaries for both Pt and Pt_3Pd_2. Atomic force microscopy (AFM) supported the observations made in the SEM micrographs, with annealing affecting the surface roughness of both thin film catalysts. These changes were quantified by determining the average surface roughness and root mean square (RMS) surface roughness (R_a and R_q, respectively) of the non-annealed and annealed Pt and Pt_3Pd_2 catalysts. The results showed that the non-annealed Pt catalyst displayed larger surface roughness parameters than Pt_3Pd_2. It was also found that annealing affected these parameters in different degrees for the two catalyst compositions, with an increase in annealing temperature resulting in an approximately linear increase in the R_a and R_q values for Pt_3Pd_2, with the lowest temperature (T_{High} = 600 °C) displaying higher values than the non-annealed catalyst. In the case of Pt, annealing at 600 and 700 °C resulted in lower values than the non-annealed catalyst, while annealing at 800 and 900 °C resulted in slightly higher (and approximately identical) surface roughness parameters when compared to the non-annealed catalyst. X-Ray diffraction (XRD) analysis revealed that annealing also had an effect on the crystallinity of the catalysts, with the crystallite size found to be significantly increased by annealing (at any temperature) for both Pt and Pt_3Pd_2 catalysts when compared to their non-annealed counterparts. The XRD data furthermore confirmed the polycrystalline nature of both catalyst compositions, and also revealed that annealing caused an increase in the degree of crystallinity for both Pt and Pt_3Pd_2.

Electrochemical experiments on the non-annealed and annealed catalyst compositions revealed that annealing (at all T_{High} points) had a negative effect on the activity of the catalysts, with both the annealed Pt and Pt_3Pd_2 thin film catalysts displaying poorer activity parameters than their non-annealed counterparts. The negative effect that annealing had on these parameters was however less significant on the Pt_3Pd_2 catalysts than on the Pt catalysts. The optimal annealing temperature (where this negative effect was the smallest) of Pt was found to be between 700 and 800 °C, with both these annealing temperatures resulting in similar activity parameters, while annealing at 600 and especially 900 °C resulted in significantly worse values. The behaviour

displayed by the annealed Pt_3Pd_2 catalysts was however quite different, with 600 and 800 °C identified as the optimal annealing temperatures as these catalysts exhibited approximately similar activity values. In this case, 700 °C was found to have the largest negative effect on the activity of the annealed Pt_3Pd_2 catalysts when compared to the non-annealed catalyst. The acid stability experiments revealed that although annealing might have a negative effect on catalyst activity it did however cause a significant increase in the stability of both Pt and Pt_3Pd_2 thin film catalysts in acidic media. For both catalysts, annealing resulted in more cycles being obtained before layer disintegration occurred when compared to the non-annealed catalysts (except for Pt 600 °C, from which 100 cycles less were obtained before the thin film catalyst layer disintegrated). As mentioned above the effect of annealing was quite significant, with the number of cycles obtained almost double for Pt (700 °C) and more than triple for Pt_3Pd_2 (800 °C) when compared to their non-annealed counterparts. Using the results obtained from the electrochemical experiments it was concluded that 800 °C was to be employed as the annealing temperature for both catalyst compositions in the RDE experiments.

RDE experiments were performed to further investigate the electrocatalytic and stability properties of the non-annealed and annealed Pt and Pt_3Pd_2 thin film catalysts. Linear polarisation (LP) was again employed to determine the kinetic properties of the catalysts through analysis of the results with various methods. While it is possible to calculate the exchange current density (i_0) of a catalyst with Levich and Koutecky-Levich analysis, it was found that this was not possible for the catalysts employed in these experiments. Due to the inhibition of SO_2 oxidation at high potentials (>1.000 V) by the formation of surface oxides, Koutecky-Levich analysis of the data could not be performed. Levich analysis of the data for the various catalysts showed that the systems were not under complete mass transport control, and thus the true limiting currents (I_L) could not be obtained. Tafel analysis of the data could however be performed successfully, with both the exchange current density and Tafel slope of the various catalysts being obtained from the analysis. While the analysis proved to be relatively time consuming due to the number of plots and calculations required, it did provide useful results which enabled a meaningful comparison of the kinetic properties of the non-annealed and annealed Pt and Pt_3Pd_2 electrocatalysts. Non-annealed Pt displayed the highest exchange current density while the annealed Pt_3Pd_2 catalyst displayed the lowest value (i_0 = 196.130 pA.cm^{-2} and i_0 = 82.410 pA.cm^{-2}, respectively). These values confirmed the conclusions made in various studies that the SDE reaction has very sluggish reaction kinetics, and thus requires large overpotentials to drive the reaction at acceptable rates. When the exchange current densities of the catalysts were compared to their activity parameters it was found that no clear correlation existed between the kinetic and activity parameter(s). However, when the Tafel slopes were included in this comparison a correlation between the kinetic and activity parameters could be seen. The catalyst with the lowest Tafel slope (non-annealed Pt_3Pd_2, b = 55.664 mV.dec^{-1}) displayed the best activity

parameters, while the catalyst with the highest Tafel slope (annealed Pt, b = 61.351 mV.dec^{-1}) displayed the poorest activity parameters. It was thus concluded that for a reaction with extremely low exchange current densities (such as SDE), the Tafel slope was the more important and useful parameter in predicting the activity that a given catalyst would display at high overpotentials.

The results obtained from the SO_2 oxidation stability experiments indicated that the non-annealed Pt thin film catalyst had the highest stability, being significantly more stable than the Pt_3Pd_2 catalyst. The annealed Pt_3Pd_2 catalyst did however display a similar degree of stability as the non-annealed Pt catalyst, while annealing had the opposite effect on Pt, with the annealed Pt catalyst being less stable than its non-annealed counterpart.

The study revealed that the binary Pt_3Pd_2 catalyst was superior to the pure Pt catalyst with regard to SO_2 oxidation activity. While the non-annealed Pt_3Pd_2 thin film catalyst displayed the best activity parameters and Tafel slope, it proved to be less stable than the non-annealed Pt catalyst. Furthermore, it was shown that while annealing does have a negative effect on the electrocatalytic activity of the Pt and Pt_3Pd_2 catalysts, the degree to which it affects both the activity and kinetic properties of the catalysts is different, with the Pt_3Pd_2 composition being much less affected. The reverse also holds true with regards to stability, with annealing increasing the stability of the Pt_3Pd_2 catalysts to a greater degree than Pt. In conclusion, it can be said that both the non-annealed and annealed Pt_3Pd_2 thin film catalysts are viable candidates to replace Pt as the catalyst of choice for SO_2 electro-oxidation.

5.2 Future recommendations

Although this study did provide useful and interesting results, it merely scratches the surface of electrocatalyst development for SO_2 electro-oxidation. Apart from the fact that other binary Pt_xM_y catalysts should be investigated, much research remains to be done on Pt_xPd_y electrocatalysts. Firstly, the surface of these sputtered thin film catalysts must be characterised in greater detail in order to gain more insight into the atomic structure and properties of the surface layer of atoms on the thin film catalysts and how they relate to the activity and stability. Since the reaction only takes place on the surface of the electrocatalyst (at active sites), understanding the effect of different catalyst deposition methods and annealing on the surface layer of atoms is very important. Furthermore, a deeper insight into the surface structure would enable the determination of the ECSA, which in turn would result in more accurate calculations of the kinetic parameters of the catalysts.

The annealing of thin film catalysts also shows promise. However, in order to fully understand the effect of annealing on the surface structure (and thus the kinetic and thermodynamic

properties of the catalyst layer) of the catalysts, annealing should be done over a greater temperature range, as well as including more temperature points (T_{High}). In the case of rapid thermal annealing, further experiments should also be conducted on the endless amount of possible temperature programs/profiles that can be created. Furthermore, different controlled cooling steps should also be included in the temperature programs, as this might have a profound effect on the final structure and properties of the catalyst layer.

Reference list

[1] United States Environmental Protection Agency. *Sulfur Dioxide*. www.epa.gov/airquality/sulfurdioxide/, Date of use : 2014/03/20.

[2] R.J. Kriek, J.P. van Ravenswaay, M. Potgieter, A. Calitz, V. Lates, M.E. Björketun, S. Siahrostan, J. Rossmeisi. *SO_2 – an indirect source of energy*. J. Southern African Mining & Metallurgy, 113 (2013), 593 – 603.

[3] J.A. O'Brien, J.T. Hinkley, S.W. Donne, S-E. Lindquist. *The electrochemical oxidation of aqueous sulphur dioxide: A critical review of work with respect to the hybrid sulphur cycle*. Electrochimica Acta, 55 (2010), 573 – 591.

[4] L. Xue, P. Zhang, S. Chen, L. Wang, J. Wang. *Sensitivity study of process parameters in membrane electrode assembly preparation and SO_2 depolarized electrolysis*. Int. J. Hydrogen Energy, (2013).

[5] K. Mazloomi, N.B. Sulaiman, H. Moayedi. *Electrical efficiency of electrolytic hydrogen production*. Int. J. Electrochem. Sci., 7 (2012), 3314 – 3326.

[6] J.M. Ogden. *Prospects for building a hydrogen energy infrastructure*. PU/CEES Report No. 318 (1999), 1 – 65.

[7] J.A. Allen, G. Rowe, J.T. Hinkley, S.W. Donne. *Electrochemical aspects of the hybrid sulfur cycle for large scale hydrogen production*. Int. J. Hydrogen Energy, 39 (2014), 11376 – 11389.

[8] P. Sivasubramanian, R. Ramasamy, F.J. Freire, C.E. Holland, J.W. Weidner. *Electrochemical hydrogen production from thermochemical cycles using a proton exchange membrane electrolyzer*. Int. J. Hydrogen Energy, 32 (2007), 463 – 468.

[9] P.W.T. Lu, R.L. Ammon. *An investigation of electrode materials for the anodic oxidation of sulfur dioxide in concentrated sulfuric acid*. J. Electrochem. Soc., 12 (1980), 2610 – 2616.

[10] P.W.T. Lu, R.L. Ammon. *Sulfur dioxide depolarized electrocatalysis for hydrogen production: Development status*. Int. J. Hydrogen Energy, 7 (1982), 563 – 575.

[11] E.T. Seo, D.T. Sawyer. *Electrochemical oxidation of dissolved sulphur dioxide at platinum and gold electrodes*. Electrochimica Acta, 10 (1965), 239 – 252.

[12] A.J. Appleby, B. Pinchon. *Electrochemical aspects of the H_2SO_4-SO_2 thermoelectrochemical cycle for hydrogen production*. Int. J. Hydrogen Energy, 01 (1980), 253 – 267.

[13] H.R. Colón-Mercado, D.T. Hobbs. *Catalyst evaluation for a sulphur dioxide-depolarized electrolyzer*. Electrochemistry Communications, 9 (2007), 2649 – 2653.

[14] J.A. O'Brien, J.T. Hinkley, S.W. Donne. *Electrochemical oxidation of aqueous sulphur dioxide II. Comparative studies on platinum and gold electrodes*. J. Electrochem. Soc., 159 (2012), 585 – 593.

[15] J.S. Cooper, P.J. McGinn. *Combinatorial screening of thin film electrocatalysts for a direct methanol fuel cell anode*. J. Power Sources, 163 (2006), 330- 338.

[16] L.E. Brecher, S. Spewock, C.J. Warde. *The Westinghouse sulfur cycle for the thermochemical decomposition of water*. Int. J. Hydrogen Energy, 2 (1977), 7 – 15.

[17] S.K. Lee, C.H. Kim, W.C. Cho, K.S. Kang, K.K. Bae. *The effect of Pt loading amount on SO_2 oxidation reaction in an SO_2-depolarized electrolyzer used in the hybrid sulfur (HyS) process*. Int. J. Hydrogen Energy, 34 (2009), 4701 – 4707.

[18] J. Lee, S.H. Langer. *Electrochemical sulphur dioxide oxidation with platinum-aluminium electrocatalysts*. J. Applied Electrochemistry, 25 (1995), 353 – 357.

[19] L. Xue, P. Zhang, S. Chen, L. Wang. *Pt-based bimetallic catalysts for SO_2-depolarized electrolysis reaction in the hybrid sulfur process*. Int. J. Hydrogen Energy, 39 (2014), 14196 – 14203.

[20] P.W.T. Lu. *Technological aspects of sulfur dioxide depolarized electrolysis for hydrogen production*. Int. J. Hydrogen Energy, 10 (1983), 773 – 781.

[21] M.B. Gorensek, J.A. Staser, T.G. Stanford, J.W. Weidner. *A thermodynamic analysis of the SO2/H2SO4 system in SO2-depolarized electrolysis*. Int. J. Hydrogen Energy, 34 (2009), 6089 – 6095.

[22] F. Jomard, J.P. Feraud, J.P. Caire. *Numerical modelling for preliminary design of the hydrogen production electrolyzer in the Westinghouse hybrid cycle*. Int. J. Hydrogen Energy, 33 (2008), 1142 - 1152.

[23] B.D. Struck, R. Junginger, H. Neumeister, B. Dujka. *Three-compartment electrolytic cell for anodic oxidation of sulfur dioxide and cathodic production of hydrogen*. Int. J. Hydrogen Energy, 7 (1982), 43 – 49.

[24] A.J. Bard, L.R. Faulkner. 2001. *Electrochemical Methods: Fundamentals and Applications.* 2nd ed. New York: John Wiley & Sons, Inc.

[25] P. Atkins, J. De Paula. 2010. *Atkins' Physical Chemistry*. 9th ed. New York: W.H. Freeman and Company.

[26] A.S. Bandarenka, E. Ventosa, A. Maljusch, J. Masa, W. Schuhmann. *Techniques and methodologies in modern electrocatalysis: evaluation of activity, selectivity and stability*. Analyst, 139 (2014), 1274 – 1291.

[27] S.A. Grigoriev, A.A. Fedetov, S.A. Martemianov, V.N. Fateev. *Synthesis of nanostructural electrocatalytic materials on various carbon subtrates by ion plasma sputtering of platinum metals*. Russian J. Electrochem., 7 (2014), 714 – 723.

[28] O.K. Alexeeva, V.N Fateev. *Application of the magnetron sputtering for nanostructured electrocatalysts synthesis*. Int. J. Hydrogen Energy, 41 (2016), 3373 – 3386.

[29] C. Quijada, J.L. Vasquez. *Electrochemical reactivity of aqueous SO_2 on glassy carbon electrodes in acidic media*. Electrochimica Acta, 50 (2005), 5449 – 5457.

[30] A. Dekanski, J. Stevanovic, R. Stevanovic, B.Z. Nikolic, V.M. Jovanovic. *Glassy carbon electrodes I. Characterization and electrochemical activation*. Carbon, 39 (2001), 1195 – 1205.

[31] J-E. Lim, J.K Kyeong Jeong, K.H. Ahn, H.J. Kim, C.S. Hwang, D-Y. Park, D-S. Lee. *Microstructural characterization of sputter-deposited Pt thin film electrode*. J. Mater. Res., 19 (2004), 460 – 468.

[32] C. Quijada, A. Rodes, J.L. Vazquez, J.M. Pérez, A. Aldaz. *Electrochemical behaviour of aqueous sulphur dioxide at polycrystalline Pt electrodes in acidic medium. A voltammetric and in-situ FT-IR study. Part II. Promoted oxidation of sulphur dioxide. Reduction of sulphur dioxide*. J. Electroanal. Chem., 398 (1995), 105 – 115.

[33] Y. Su, M. Feng, C. Zhang, Z. Yan, H. Liu, J. Tang, H. Du. *Platinum Nanowires: Structural and catalytic evolution upon annealing temperature*. Electrochimica Acta, 164 (2015), 182 – 186.

[34] J.S. Cooper, P.J. McGinn. *Combinatorial screening of fuel cell cathode catalyst compositions*. Appl. Surf. Sci., 254 (2007), 662 - 668.

[35] M. Raposo, Q. Ferreira, P.A. Ribeiro. *A Guide for Atomic Force Microscopy Analysis of Soft-Condensed Matter*. Modern Research and Educational Topics in Microscopy, 1 (2007), 758 – 769.

[36] S.E. Oraby, A.M. Alaskari. *Atomic Force Microscopy (AFM) Topographical Surface Characterisation of Multilayer-Coated and Uncoated Carbide Inserts*. Int. J. Mech., Aerospace, Industrial, Mechatronic, and Manufacturing Engineering, 10 (2010), 977 – 988.

[37] D.A.J. Rand, R. Woods. *A study of the dissolution of platinum, palladium, rhodium and gold electrodes in 1 M sulphuric acid by cyclic voltammetry*. J. Electroanal. Chem. And Interfacial Electrochem., 35 (1972), 209 - 218.

[38] B.R. Shresta, A. Nishikata, T. Tsuru. *Channel flow double electrode study on Pd dissolution during potential cycling in sulfuric acid solution*. Electrochimica Acta, 70 (2012), 42 - 49.

[39] J.F. Llopis, M.M. Gamboa, L. Victori. *Radiochemical study of the anodic behaviour of palladium*. Electrochima Acta, 17 (1972), 2225 - 2230.

[40] A.J. Appleby, B. Pinchon. *The mechanism of the electrochemical oxidation of sulfur dioxide in sulfuric acid solutions*. J. Electroanal. Chem., 95 (1979), 59 – 71.

[41] D. Pletcher. 2009. *A First Course in electrode processes*. 2nd ed. United Kingdom: Royal Society of Chemsitry.

[42] J.A. O'Brien, J.T. Hinkley, S.W. Donne. *The Electrochemical Oxidation of Aqueous Sulfur Dioxide: I. Experimental Parameter Influences on Electrode Behaviour*. J. Electrochem. Soc., 157 (2010), 111 – 115.

Appendix

Table 1: Regression lines for Tafel analysis of non-annealed Pt with coefficients of determination, slopes, intercepts and the calculated values of exchange current densities and Tafel slopes

	R^2	Intercept	Slope	Exchange current density ($pA.cm^{-2}$)	Tafel slope ($mV.dec^{-1}$)
Set 1	0.994	-7.3647	0.0172	219.923	58.140
Set 2	0.987	-7.5107	0.0168	157.134	59.524
Set 3	0.900	-7.3820	0.0171	211.334	58.480
Average	0.960			196.130	58.714
Std.Dev.	0.053			34.044	0.721

Table 2: Regression lines for Tafel analysis of annealed Pt with coefficients of determination, slopes, intercepts and the calculated values of exchange current densities and Tafel slopes

	R^2	Intercept	Slope	Exchange current density ($pA.cm^{-2}$)	Tafel slope ($mV.dec^{-1}$)
Set 1	0.953	-7.6553	0.0164	112.634	60.976
Set 2	0.998	-7.6900	0.0163	103.985	61.350
Set 3	0.981	-7.5430	0.0162	148.926	61.728
Average	0.977			121.848	61.351
Std.Dev.	0.022			23.845	0.376

Table 3: **Regression lines for Tafel analysis of non-annealed Pt_3Pd_2 with coefficients of determination, slopes, intercepts and the calculated values of exchange current densities and Tafel slopes**

	R^2	Intercept	Slope	Exchange current density ($pA.cm^{-2}$)	Tafel slope ($mV.dec^{-1}$)
Set 1	0.916	-7.6710	0.0178	108.635	56.180
Set 2	0.987	-7.7752	0.0182	85.461	54.945
Set 3	0.959	-7.6879	0.0179	104.489	55.866
Average	0.954			99.528	55.664
Std.Dev.	0.036			12.358	0.642

Table 4: **Regression lines for Tafel analysis of annealed Pt_3Pd_2 with coefficients of determination, slopes, intercepts and the calculated values of exchange current densities and Tafel slopes**

	R^2	Intercept	Slope	Exchange current density ($pA.cm^{-2}$)	Tafel slope ($mV.dec^{-1}$)
Set 1	0.972	-7.7767	0.0169	85.167	59.172
Set 2	0.980	-7.7687	0.0168	86.750	59.524
Set 3	0.947	-7.8301	0.0169	75.313	59.172
Average	0.967			82.410	59.289
Std.Dev.	0.017			6.197	0.203